REVIEW

Chinese Journal of Structural Chemistry

# Research Progress of Ferrite Materials for Photoelectrochemical Water Splitting

Yani Wang[1], Jingwei Huang[1], Lei Wang[1], Houde She[1] and Qizhao Wang[1,2,3]*

[1]*College of Chemistry and Chemical Engineering, Gansu International Scientific and Technological Cooperation Base of Water-Retention Chemical Functional Materials, Northwest Normal University, Lanzhou 730070, China*

[2]*School of Environmental Science and Engineering, Chang'an University, Xi'an 710054, China*

[3]*Tianjin Key Laboratory of Building Green Functional Materials, Tianjin Chengjian University, Tianjin 300384, China*

**ABSTRACT** Photoelectrochemical (PEC) water splitting is an effective strategy to convert solar energy into clean and renewable hydrogen energy. In order to carry out effective PEC conversion, researchers have conducted a lot of exploration and developed a variety of semiconductors suitable for PEC water splitting. Among them, metal oxides stand out due to their higher stability. Compared with traditional oxide semiconductors, ferrite-based photoelectrodes have the advantages of low cost, small band gap, and good stability. Interestingly, due to the unique characteristics of ferrite, most of them have various tunable features, which will be more conducive to the development of efficient PEC electrode. However, this complex metal oxide is also troubled by severe charge recombination and low carrier transport efficiency, resulting in lower conversion efficiency compared to theoretical value. Based on this, this article reviews the structure, preparation methods, characteristics and modification strategies of various common ferrites. In addition, we analyzed the future research direction of ferrite for PEC water splitting, and looked forward to the development of more efficient catalysts.

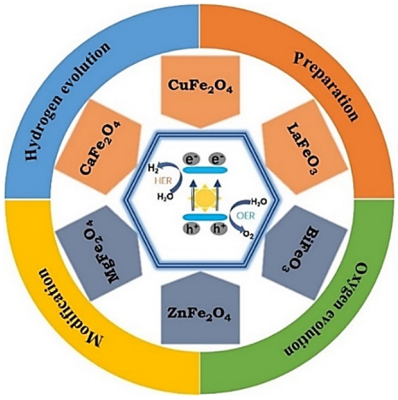


**Keywords:** ferrite, photoelectrochemical, water splitting, hydrogen

## n INTRODUNTION

With the continuous development of society, the dual pressure of energy and environment makes people have to pay attention to the use of clean energy. Solar energy is a huge clean energy source that can be used to convert some of the earth's rich substances, such as $CO_2$,[1,2] $H_2O$,[3-5] $N_2$[6,7] etc, into high-value-added product.[8-10] Among them, photoelectrochemical (PEC) water splitting has become one of the most promising methods to convert solar energy into clean and renewable hydrogen energy since it was discovered by Fujishima and Honda in 1972.[11-13] In the PEC water splitting, semiconductor absorbs light to generate electron-hole pairs, which then separate and transport to the electrode surface to undergo reduction and oxidation reactions, respectively.[14,15] Therefore, the development of high-efficiency semiconductors is a key part of improving the efficiency of PEC water splitting. There are two types of photoelectrodes that can be used for PEC water splitting. N-type semiconductors are commonly used for photoanodes. For example, ZnO,[16,17] $BiVO_4$,[18-21] $TiO_2$,[2,22] $Fe_2O_3$,[23,24] $WO_3$,[25-28] etc. P-type semiconductors such as $CuFe_2O_4$,[29] CuO,[30] $BiFeO_3$[31,32] and so on are used for the photocathode. Generally speaking, an efficient PEC water splitting system can include both a photoanode and a photocathode (Figure 1c).[33] However, due to many factors that need to be considered in series electrodes, the most researched PEC water splitting system is a single photoanode or photocathode. In this system, the photoanode undergoes oxidation reaction and the photocathode undergoes reduction reaction. When the semiconductor electrode is immersed in the electrolyte, the system will cause the energy band of the semiconductor to be bent in order to maintain the electrostatic balance. The schematic diagrams of the p-type photocathode and n-type photoanode in the electrolyte are shown in Figure 1a and 1b.

Previous studies have found that semiconductors that can achieve unassisted PEC water splitting should have the following characteristics: (1) Appropriate band gap energy.[34] Due to the activation barrier between the catalyst and water molecules, the band gap energy of the semiconductor must be greater than the dissociation energy of water (1.23 eV). (2) The conduction band and valence band of the semiconductor should cross the redox potential of water, that is, the conduction band position of semiconductor is more negative than the water reduction potential (0 V vs. RHE), and the valence band position is more positive than the water oxidation potential (1.23 V vs. RHE). (3) Efficient charge mobility and long carrier diffusion length. (4) Good stability, abundant earth reserves, and low cost. Oxide-based photoelectrodes stand out among many photoelectrode semiconductors used for PEC water splitting due to their suitable band gap, good stability in electrolytes, and low cost, which has attracted wide attention from researchers.[35-37] However, early research on oxide semiconductors focused on simple binary oxides, such as $TiO_2$,[38] $Fe_2O_3$,[39] ZnO,[16] CuO,[30] $WO_3$[26,27] and so on. In recent studies, people have found that the ternary oxide formed by the combination of two metal ions has many unique structural properties, such as ferroelectricity, superconductivity, phase change, etc., which make the ferrite more promising for PEC water splitting. In the comprehensive evaluation of excellent photoelectric catalytic semiconductors, it is not only necessary to have high photoelectric conversion efficiency, but also to consider the cost of large-scale application. Generally speaking, the preparation cost of ferrite materials is low. It has a suitable band gap that is conducive to more visible light absorption, and has good stability to various alkaline or acidic media in the water decomposition process. In addition, ferrite materials can also be used as auxiliary catalysts

  

DOI: 10.14102/j.cnki.0254-5861.2021-0020

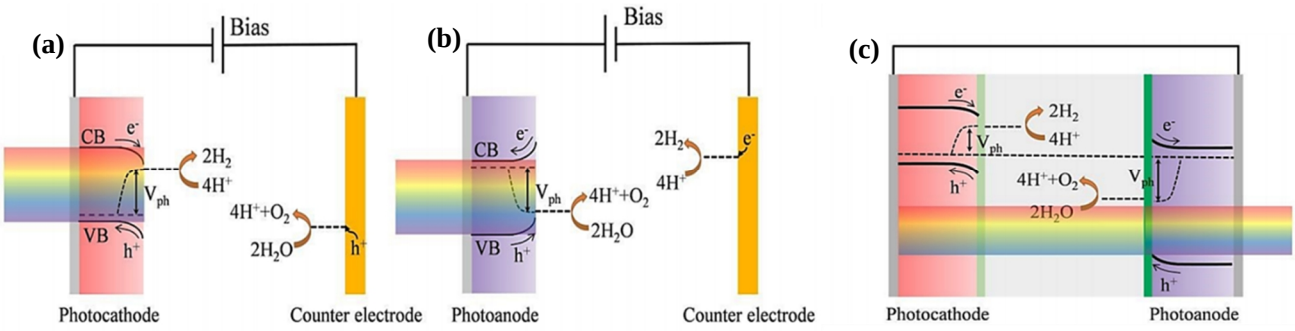


**Figure 1.** (a) Principle of operation of PEC cells based on bias-assisted p-type semiconductor, (b) Bias-assisted n-type semiconductor, and (c) Bias-free tandem structure consisting of p-type and n-type photoelectrodes. Reproduced with permission from Ref.[33]

to improve the PEC performance of other semiconductors. The multi-functionality and tunable structure of ferrite materials provide many opportunities for designing high-efficiency water splitting catalysts. However, ferrite still exhibits low photoelectric conversion efficiency when applied to photoelectrodes, which is due to the severe sintering of ferrite and rapid charge recombination. Therefore, various strategies have been developed to optimize ferrites.

This article reviews the structure, preparation and modification strategies of common n-type and p-type ferrites, analyzes the bottleneck of ferrite used in PEC water splitting, and looks forward to its future research directions (Figure 2).

## n THE STRUCTURE OF FERRITE

Ferrite is a kind of magnetic oxide with iron oxide ($Fe^{3+}{}_2O_3$) as the main component. It generally contains $Fe^{3+}$ and at least another metal cation. According to their crystal structure, they can be roughly divided into six types: spinel type, perovskite type, garnet type, magnetoplumbite type, ilmenite type and tungsten bronze type. Spinel and garnet ferrite crystallize in cubic structure, while magnetoplumbite and perovskite types crystallize in hexagonal and square structures, respectively. The most commonly used ferrites in PEC water splitting are the first two types.

**Spinel Ferrite.** Spinel ferrite is a compound with a general chemical formula of $MFe_2O_4$, where M is a divalent metal cation, and its crystal structure is the same as that of the naturally occurring mineral spinel $MgAl_2O_4$ ($AB_2O_4$ is a general component).[35] The spinel crystal structure belongs to the cubic Fd3m space group. A unit cell of spinel ferrite has 56 ions, including 32 oxygen anions, 8 $M^{2+}$ cations and 16 $Fe^{3+}$ cations (Figure 3). Because oxygen ions are relatively large and metal ions are generally small, oxygen ions can be regarded as being arranged in a cubic close-packed form, and metal ions are filled in close-packed voids. Because there are two different valence cations (+2 and +3) available, there are two types of close-packed voids, namely octahedral voids and tetrahedral voids. The tetrahedral void is surrounded by four oxygen ions, called the "A" position, and the octahedral void is surrounded by six oxygen ions, called the "B" position.[40,41] In a spinel unit cell, there are 8 metal ions M occupying the A site (also called 8a) and 16 metal ions Fe occupying the B site, and the remaining gaps are vacancies, which are affected by factors such as ion valence and balance. It is worth mentioning that this vacancy is conducive to the substitution of other metal ions, which also provides a favorable basis for the doping modification of ferrite, so that it can be widely used in different fields.

**Perovskite Type Ferrite.** Perovskite originally refers to a mineral with the chemical formula $CaTiO_3$, and later is used to refer to all $ABX_3$ type substances. Its structure is shown in Figure 4. Metal ions with a relatively large ion radius are easier to occupy the A site, and they are located at the apex of the cube; the variable valence transition element Fe ion has a relatively small radius and is easier to occupy the B site. Oxygen ions are located in the center of the six faces of the cube, and it forms an octahedron with $Fe^{3+}$. Among them, the A and B sites can be fully or partially replaced by doping with ions close to their radius to change the original element valence or change the number of oxygen vacancies contained in the crystal grains, thereby changing the properties of the material.[36]

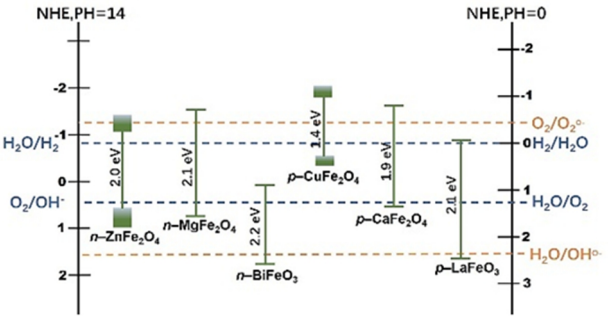


**Figure 2.** Band positions of the most popular spinel ferrites in contact with aqueous solution referenced to normal hydrogen electrode (RHE) (right pH 0 and left pH 14) relative to the standard potentials for the oxidation and reduction of water.

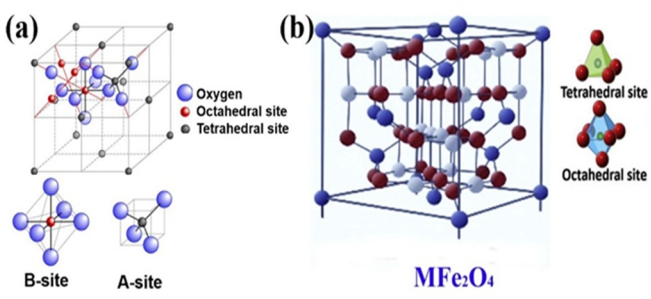


**Figure 3.** Spinel ferrite cell structure as reported by (a) Özgur et al. Reproduced with permission from Ref.[40], and (b) Amiri et al. Reproduced with permission from Ref.[42]

  

DOI: 10.14102/j.cnki.0254-5861.2021-0020

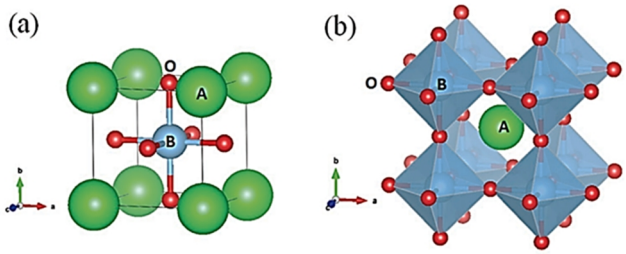


**Figure 4.** Two alternative settings of the cubic aristo type of the $ABO_3$ perovskite: (a) B-site cation at the center of the cell. (b) Corner-sharing ($BO_6$) octahedra with A ions located in 12-coordinated interstices. Reproduced with permission from Ref.[36]

## n PREPARATION METHOD

The preparation method of a compound determines its performance to a large extent. The structure, specific surface area, and particle size of the substances produced by different preparation methods are different, resulting in different properties of the substance.[43-46] There are many known preparation methods of ferrite. The commonly used methods are sol-gel method,[47] pulsed laser deposition,[48] hydrothermal method,[49] template method,[50] and the like.

**Spray Pyrolysis Method.** The spray pyrolysis refers to spraying the metal salt solution into a high temperature atmosphere in the form of a mist, causing the evaporation of the solvent and the thermal decomposition of the metal salt, and then the solid phase is precipitated due to supersaturation, thereby directly obtaining the nano powder.[51,52] Although the equipment and process of the spray pyrolysis method are simple, it can also grow excellent films comparable to other methods, and is easy to achieve doping. It is a very economical film preparation method and is expected to achieve large-scale production. Li[53] et al. prepared a pure and $Ti^{4+}$ doped $ZnFe_2O_4$ photoanode by a fast and effective spray pyrolysis method. The phase composition of $ZnFe_2O_4$ was confirmed by XRD and transmission electron microscopy. This material has excellent PEC stability in 1M NaOH. Chen[54] et al. briefly reviewed the use of flame spray pyrolysis to prepare various transition metal oxides and apply them to photoelectric catalytic water splitting. When the flame nozzle is adjusted to an appropriate angle, the flame spray pyrolysis method can be used to directly prepare various heterogeneous oxides. This method is expected to be an effective preparation method for complex ferrite photoelectric thin films.

**Sol-gel Method.** The sol-gel method is widely used to prepare ferrite.[47,55-57] The method requires mild preparation conditions, low processing temperature, and easy control of the reaction. It is an indispensable method for preparing thin film materials, which has been reported so far. The organic or inorganic salt is used as a precursor to dissolve in a certain amount of water or an organic solvent in proportion. A complexing agent is added to cause a complexation reaction to form a sol. Finally, the water or the organic solvent is removed by drying and calcining to obtain a crystalline state film.[47]

Benaissa et al. synthesized nanoporous $LaFeO_3$ powders using an ascorbic acid-assisted sol-gel method.[58] In order to verify whether the generation of porous structure can provide more reaction sites and improve photocatalytic activity, experiments demonstrated the use of ascorbic acid-assisted sol-gel technology does introduce high-density pores in nanoparticles, which widens the band gap energy of the nanoparticles, thus providing a large number of candidate materials for solar photocatalytic applications. Triyono et al. successfully obtained orthogonal single-phase $LaFe_{1-x}Mg_xO_3$ ($x$ = 0.1, 0.2 and 0.3) nanoparticles using the sol-gel method, and studied the effect of magnesium substitution on the Fe site of perovskite-type $LaFeO_3$.[47] The characterization shows that the resulting compound has a high specific surface area, resulting in a powder size of 40–130 nm.

**Hydrothermal Method.** Hydrothermal method refers to a method in which water is used as a solvent, a supersaturated solution of powder is added to a high-pressure reaction kettle, and the reaction is performed under high temperature and pressure conditions, followed by separation, washing, and drying.[59-62] That used raw materials are usually lower cost while obtained product has good crystallinity, fine particle size, good dispersibility, and uniform size.[63] Dang et al. successfully prepared Ce-doped spinel $CuFe_2O_4$ powder by a hydrothermal method. The collected nanoparticles were observed and analyzed by basic characterization methods. The results show that the sample has a small particle size and a suitable band gap structure, good crystallinity and uniform growth.[64]

Because the solvent used in the hydrothermal synthesis method is water, if the produced substance is a water-soluble compound, it will no longer be applicable, which limits the further development of this method. Therefore, a solvothermal synthesis method was developed later. It differs from the hydrothermal method in which the solvent used is an organic solvent instead of water. The process is relatively simple and easy to control, and it can effectively prevent toxic substances in a closed system. By volatilization and preparation of air-sensitive precursors, Li et al. successfully synthesized a novel p-n $LaFeO_3$/g-$C_3N_4$ heterojunction photocatalyst by a simple solvothermal method.[65] Compared with the original $LaFeO_3$ and g-$C_3N_4$, $LaFeO_3$/g-$C_3N_4$ sample has more excellent photocatalytic activity and stability.

**Pulsed Laser Deposition.** Pulsed laser deposition (PLD) is the use of a laser to bombard an object and then deposit the bombarded material on different substrates to obtain a precipitation or thin film.[48,50,66-69] Marschall et al. prepared phase-pure spinel $ZnFe_2O_4$ and $MgFe_2O_4$ thin film photoanodes through PLD.[70] The thin film structure prepared by this method is highly efficient and dense, non-nano-structured, so that it is not subject to surface effects when performing electronic and photoelectrochemical properties. The method can also be extended to the preparation of other complex metal semiconductors to study the transport characteristics of carriers, light absorption and chemical stability. Choi et al. prepared a high specific surface area nanoporous $LaFeO_3$ photocathode by a nitrate reduction electrochemical co-deposition method and tested its photocatalytic water reduction and $O_2$ reduction performance.[71] The prepared $LaFeO_3$ film has high crystallinity, uniform film formation, and good photo-corrosion resistance.

**Template Method.** Nanomaterials with special morphology sometimes need to be obtained during the material preparation process.[72-74] Generally, template synthesis is used to prepare the template. The method deposits relevant materials into the holes or surfaces of the template, and then removes the template by a certain method, so as to obtain nano-materials with the standardi-

  
DOI: 10.14102/j.cnki.0254-5861.2021-0020

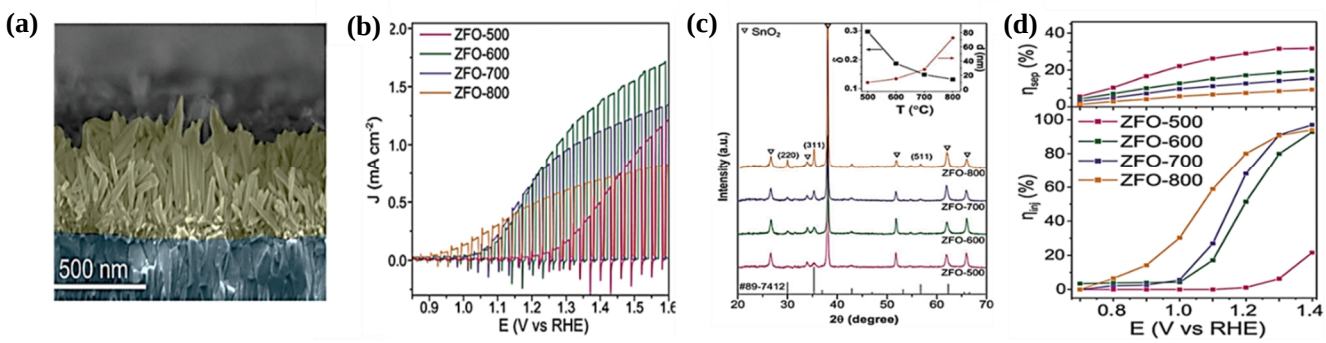


**Figure 5.** (a) Scanning electron microscopy images of the *β*-FeOOH nanorod array precursor films. (b) *J*-*V* curves. (c) XRD patterns of $ZnFe_2O_4$ nanorod array photoelectrodes prepared on FTO coated glass are shown with the reference pattern for ZFO. (d) Estimated charge separation efficiency, and minority charge carrier injection efficiency. Reproduced with permission from Ref.[81]

zed morphology and size of the template.[75-77]

Marschall et al. used a simple, fast, one-step soft template method, self-assembly to synthesize pure phase $NiFe_2O_4$ powder for electrocatalytic oxygen generation.[78] Different pore diameters can be formed at different calcination temperatures, so that the $NiFe_2O_4$ nanostructure has adjustable surface area, pores and crystallinity, thereby affecting the electrocatalytic performance.

Fu et al. successfully prepared nanometer $LaFeO_3$ using mesoporous silica SBA-16 as a hard template.[79] After calcination at 800 °C, it still has a larger surface area of 85 $m^2 \cdot g^{-1}$. The surface area of $LaFeO_3$ prepared by the method is much larger, and it has higher visible activity after calcination at high temperature. Recently, Jing et al. have successfully prepared egg yolk shell-type $LaFeO_3$ nanospheres by the template method.[74] Compared with pure bare $LaFeO_3$ nanoparticles, the visible light activity of yolk shell-type $LaFeO_3$ microspheres for 2,4-DCP degradation is significantly improved. This study provides a feasible strategy for the synthesis of morphology-based photocatalysts for environmental remediatio

## n FERRITE USED FOR PEC WATER SPLITTING

### Ferrite Photoanode for Water Oxidation

**$ZnFe_2O_4$.** Spinel $ZnFe_2O_4$ is composed of environment-friendly and earth-rich elements. It has high photocatalytic activity and is sensitive to visible light. Its band gap is about 2.0 eV, and its narrow energy gap makes it excellent for visible light collection. The valence band maximum of $ZnFe_2O_4$ is slightly higher than the oxidation potential of water. This series of characteristics makes $ZnFe_2O_4$ thermodynamically more suitable for PEC water splitting. However, poor conductivity and slow water oxidation kinetics hinder its application to a large extent, making $ZnFe_2O_4$ as a single photoanode be rarely reported. So far, the photocurrent of $ZnFe_2O_4$ used for water splitting is still far below its theoretical value. Therefore, it is still a major challenge to develop effective modification methods to improve the PEC performance of spinel $ZnFe_2O_4$. Researchers have explored many methods to solve these limitations. For example, ion doping is used to improve the conductivity of $ZnFe_2O_4$, while heterostructures such as $ZnFe_2O_4$/ZnO and $TiO_2$/$ZnFe_2O_4$ are constructed to enhance interfacial charge transfer. As mentioned earlier in the article, the formation of spinel ferrite films generally requires stricter temperature control. Conventional high-temperature annealing may damage the transparent conductive substrate. Lee and colleagues used a full-solution method to prepare one-dimensional $ZnFe_2O_4$ nanorods on FTO substrates.[80] Different annealing conditions were used for comparison: conventional thermal annealing (CTA; 550, 800 °C) and hybrid microwave annealing (HMA). The results show that external doping mainly promotes the increase of charge density and charge transport, thereby increasing the bulk charge separation efficiency. Sivula et al. synthesized spinel $ZnFe_2O_4$ by calcination at different temperatures to convert *β*-FeOOH on F-doped tin oxide (FTO) glass substrate.[81] SEM (Figure 5a) and XRD tests proved the formation of $ZnFe_2O_4$ with different morphologies and crystallinity at different temperatures (Figure 5c). The results show that $ZnFe_2O_4$ nanorod array photoelectrodes with different crystallinity exhibit significantly different PEC characteristics, and the solar photocurrent can reach up to 1.0 $mA \cdot cm^{-2}$ at 1.23 V vs. RHE (Figure 5b). The author also found that different synthesis temperatures will affect the crystallinity and cation disorder of the spinel structure, thus affecting the charge separation and injection characteristics of the electrode (Figure 5d).

Recently, Sang et al. calcined $ZnFe_2O_4$ for different time at the same temperature and used $NaH_2PO_2$ for phosphating.[82] PEC performance tests and DOS calculations showed that the formed $ZnFe_2O_4$ had different crystallinity and oxygen vacancies. This improved the ferromagnetism and intrinsic electronic structure energy. The formation of spin polarization in a specific magnetic field induces and inhibits the charge recombination. Ferromagnetism is a common feature of most ferrite materials. This research provides a new idea for other materials, which enhances the performance of PEC by adjusting the internal electronic structure to enhance the polarization characteristics of the magnetic field.

In the research of photoelectric catalysis, improving the conductivity of the material is another effective measure to enhance its PEC performance. Qin and colleagues synthesized pure and titanium-doped $ZnFe_2O_4$ photoanode for the first time, and discussed the effect of different ion doping concentrations on the PEC performance of photoelectrode.[83] The results show that the material has excellent PEC stability in 1 M sodium hydroxide. In addition, titanium ion doping significantly increases the photocurrent, which can be attributed to the enhanced conductivity and carrier transport.

In addition, because the photocurrent density of single $ZnFe_2O_4$ is far lower than its theoretical value, there are few reports about single $ZnFe_2O_4$ as a photoanode, but it is used as an auxiliary-catalyst to form heterojunctions with other materials, which bene-

  
DOI: 10.14102/j.cnki.0254-5861.2021-0020

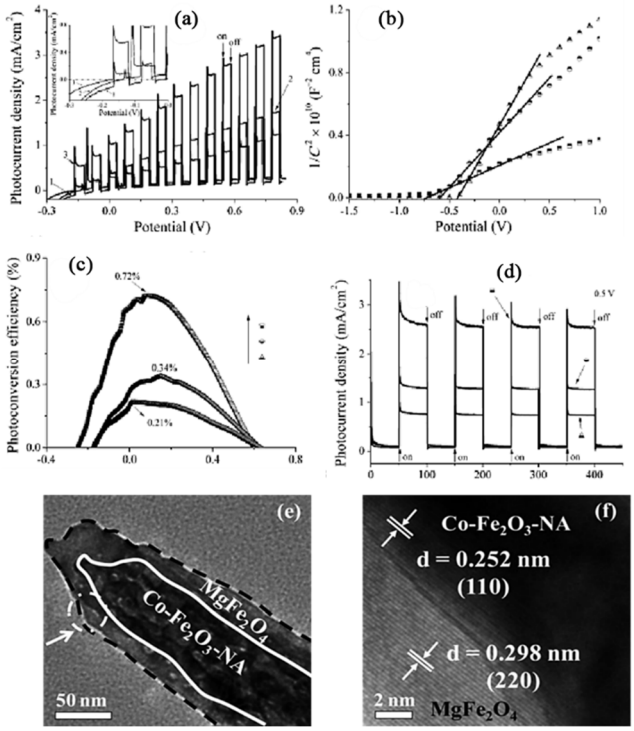


**Figure 6.** (a) Variation of photocurrent density versus applied voltage. (b) Mott-Schottky plots. (c) Photoconversion efficiency as a function of applied potential, and (d) transient photocurrent density versus time plotted for $Fe_2O_3$-NA (1,△), Co-$Fe_2O_3$-NA (2,○), and Co-$Fe_2O_3$-NA/$MgFe_2O_4$ heterojunction (3,□). HRTEM images of the Co-$Fe_2O_3$-NA/$MgFe_2O_4$ heterojunction (e and f). Reproduced with permission from Ref.[88]

fits from the stable $ZnFe_2O_4$ characteristics and suitable band gap. Many studies have shown that combining $ZnFe_2O_4$ with other wide band gap semiconductors can effectively enhance visible light absorption. Chen et al. prepared a tightly arranged $ZnFe_2O_4$/$TiO_2$ composite nanotube array.[84] The absorption of the composite nanotube array in the ultraviolet and visible regions is enhanced, and the formation of heterojunction enhances the separation of photogenerated electrons and holes. Wang and his colleagues synthesized ZnO/ $ZnFe_2O_4$ heterojunction, and used it as a photoanode for water splitting to produce hydrogen.[85] The load of corrugated $ZnFe_2O_4$ on the one hand provides a larger surface area, which increases the number of active sites and enhances the absorption of visible light. On the other hand, it forms a heterojunction with ZnO to promote the separation of electrons and holes. This research provides new ideas for using other ferrites with specific morphologies to modify photoelectrode materials.

In summary, researchers have explored a variety of modification strategies to continuously improve the PEC performance of $ZnFe_2O_4$ from various aspects such as controlling film formation conditions, improving charge transport, and improving water oxidation kinetics. If the unique electromagnetic structure of the body is to be used as an effective photoanode, the key future research task should pay more attention to the exploration of structural characteristics and combine multiple modification methods.

**$MgFe_2O_4$.** Spinel $MgFe_2O_4$ is an n-type oxide with low cost, environmental friendliness, wide spectral response, good stability, and light corrosion resistance. Its band gap is 2.0–2.2 eV. The appropriate energy band position makes $MgFe_2O_4$ as a promising photocatalyst. However, there have been few studies on its performance as a PEC water splitting photoanode so far. The main obstacle is its poor electrical conductivity and fast charge carrier recombination. At present, researchers have adopted a variety of modification methods to improve the PEC water splitting performance of $MgFe_2O_4$. First of all, the structure of $MgFe_2O_4$ is a twisted cubic spine, and the preparation process can greatly affect the degree of inversion. Bartlett et al. used a rapid microwave heating and annealing method to prepare nanocrystalline $MgFe_2O_4$.[86] The study found that the annealing temperature can affect the degree of reversal of the positions of Mg and Fe, thereby affecting the optics, electronics and composition of the nanoparticles.

In addition, the heterojunction structure has been extensively studied and can be used to accelerate electron and hole transport and inhibit charge recombination.[87] As early as 2013, Feng and colleagues proposed a 3D branch heterojunction as a photoanode for PEC water oxidation.[88] This 3D structure has a larger surface area, better charge transport and more effective light absorption characteristics (Figure 6e and f). The PEC performance test of 3D Co-$Fe_2O_3$-NA/$MgFe_2O_4$ heterojunction showed photocurrent density (3.34 mA·cm$^{-2}$) higher than Co-$Fe_2O_3$-NA (1.71 mA·cm$^{-2}$) and pure $MgFe_2O_4$ (0.39 mA·cm$^{-2}$) (Figure 6a and d).

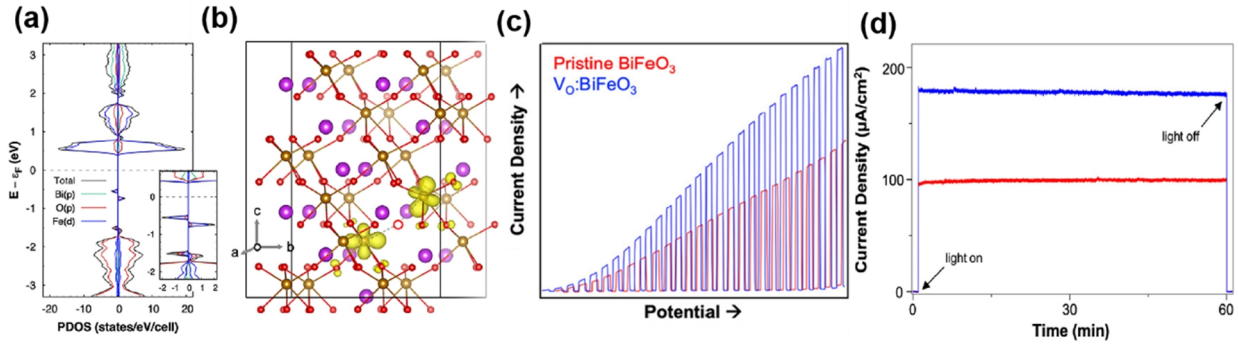


**Figure 7.** (a) Projected density of states (PDOS) for $BiFeO_3$ with a single oxygen vacancy (VO) introduced into a 120-atom supercell. (b) Norm-squared wave function of the two electron-polarons (yellow regions surrounding Fe). Isosurface value is 1% of the maximum amplitude of the wave function. VO is indicated by a single empty red circle between the two electron-polarons. (c) J−V plots and (d) J−t plots at 0.8 V vs RHE for pristine $BiFeO_3$ (red) and $N_2$-treated $BiFeO_3$ (blue) for sulfite oxidation. Reproduced with permission from Ref.[94]

  

DOI: 10.14102/j.cnki.0254-5861.2021-0020

**Table 1.** Comparison of PEC Performance, Onset Potential and Preparation of Different Ferrite Photoanode for Water Oxidation

| Ferrite photoanode | Electrolyte | $J$ (1.23 V vs RHE) | $V_{onset}$ ($V_{RHE}$) | Preparation | Reference |
|---|---|---|---|---|---|
| Bare $ZnFe_2O_4$ | 1 M NaOH | 0.56 mA·cm$^{-2}$ | 0.9 | hydrothermal | [98] |
| $ZnFe_2O_4$ | 1 M NaOH | 0.01 mA·cm$^{-2}$ | 1.0 | all-solution method | [99] |
| $ZnFe_2O_4$ | 1 M NaOH | 0.02 mA·cm$^{-2}$ | 1.0 | spin-coating method | [83] |
| $(Zn_{1-x}Fe_x)Fe_2O_{4-y}$ | 1 M NaOH | 0.22 mA·cm$^{-2}$ | 0.8 | spin-coating method | [83] |
| $ZnO/ZnFe_2O_4$ | 0.25 M $Na_2SO_3$ and 0.35 M $Ns_2S$ | 1.3 mA·cm$^{-2}$ at 0 V vs Ag/AgCl | –0.5 V vs Ag/AgCl | electrodeposition | [85] |
| Cu,Sn-$ZnFe_2O_4$ | 0.5 M $Na_2SO_4$ | 0.46 mA·cm$^{-2}$ | 0.85 | hydrothermal method | [43] |
| $ZnFe_2O_4$ | 1 M NaOH | 1.0 mA·cm$^{-2}$ | 1.0 | chemical bath deposition | [81] |
| Ti (6%) $ZnFe_2O_4$ | 1 M NaOH | 0.35 mA·cm$^{-2}$ | 0.95 | spray pyrolysis method | [53] |
| $MgFe_2O_4$ | 1 M NaOH | 26.1 mA·cm$^{-2}$ at 1.5 V vs RHE | 1.0 | pulsed laser deposition | [70] |
| Co-$Fe_2O_3$-NA/ $MgFe_2O_4$ | 0.01M $Na_2SO_4$ | 2.55 mA·cm$^{-2}$ at 1.1 V vs RHE | 0.43 | hydrothermal deposition | [88] |
| $MgFe_2O_4$ | 1 M NaOH | 4.3 μA·cm$^{-2}$ | 0.7 | solution method | [100] |
| $WO_3/BiFeO_3$ | 0.5 M $Na_2SO_4$ | 35.2 mA·cm$^{-2}$ at 2 V vs Ag/AgCl | 1.01 | sol-gel spin coating | [101] |
| $BiFeO_3$ | 0.1 M $Na_2SO_4$ | 0.23 mA·cm$^{-2}$ at 1.0 V vs Ag/AgCl | 0.6 | facile ultrasonic/hydrothermal | [31] |
| Ag:$BiVO_4/BiFeO_3$ | 0.1 M $Na_2SO_4$ | 0.72 mA·cm$^{-2}$ | 0.6 | spin coating | [102] |
| $N_2$-treated $BiFeO_3$ | 0.25 M $H_3BO_3$ and 0.7 M $Na_2SO_3$ | 440 μA·cm$^{-2}$ | 0.38 | electrodeposition | [94] |
| $BiFeO_3$ | 1 M NaOH | 28.75 mA·cm$^{-2}$ at 1.5 V vs SCE | 0.5 V vs SCE | sol-gel process | [103] |
| $WO_3/BiVO_4$/ $BiFeO_3$ | 0.5 M $Na_2SO_4$ | 46.9 mA·cm$^{-2}$ at 2.53 V vs RHE | 0.7 | sol preparation | [104] |
| $BiFeO_3$ | 0.5 M $Na_2SO_4$ | 0.08 mA·cm$^{-2}$ at 0 V vs Ag/AgCl | 0.38 | solid-state reaction method | [32] |

The results show that the impurity level formed by the co-doping method promotes the charge transfer efficiency (Figure 6c). The formation of a heterojunction structure reduces the recombination of photogenerated electron-hole pairs. The effective separation of photogenerated electron-hole pairs is essential to enhance the PEC activity. So far, a variety of heterojunction structures have been studied and reported, such as Z-type $MgFe_2O_4/Bi_2MoO_6$ heterojunction[89] and $MgFe_2O_4/MoS_2$ heterojunction.[90]

Previous studies have proved that ion doping can actually enhance the conductivity of semiconductors. Batoo et al. prepared $Cd^{2+}$ doped $MgFe_2O_4$ nano ferrites using citrate gel autooxidation technology.[91] The doping of $Cd^{2+}$ ions increased the particle and lattice parameters. FTIR studies confirm that $Cd^{2+}$ ions are more inclined to the (A) site of the tetrahedron. The doped $MgFe_2O_4$ has higher electrical conductivity, which is higher than that for other current nano ferrites. Ilanchezhiyan et al. prepared a new type of Zn ion doped $MgFe_2O_4$ nanospheres for the first time.[92] The results show that Zn doping can increase the conductivity of $MgFe_2O_4$ and accelerate the charge transfer. The doped $MgFe_2O_4$ nanostructures show higher photocatalytic activity and enhanced photocurrent density than the original $MgFe_2O_4$. In short, due to the similar structural characteristics of $ZnFe_2O_4$ and $MgFe_2O_4$, the modification strategy of $ZnFe_2O_4$ mentioned above can still be used to modify $MgFe_2O_4$. The most noteworthy problem of $MgFe_2O_4$ is the serious charge recombination. Future research should focus on improving the surface and increasing the power of water oxidation.

**$BiFeO_3$.** Perovskite structure $BiFeO_3$ has a large ferroelectric effect, and has been reported as a ferroelectric diode device, one of the most promising candidate devices for the PEC water splitting. The band gap of $BiFeO_3$ is about 2.2 eV, which is conducive to visible light absorption. The minimum value of the conduction band (CBM) and the maximum value of the valence band (VBM) span the redox potential of the entire water splitting.[93] Interestingly, in the absence of an external doping source, it is easy to form both n-type and p-type $BiFeO_3$ by own vacancies, such as oxygen vacancies can lead to n-type $BiFeO_3$, and Bi vacancies can cause p-type $BiFeO_3$. Choi et al. prepared a highly uniform $BiFeO_3$ photoanode by a simple electrodeposition method, and heat-treated it in a $N_2$ atmosphere to make it rich in oxygen vacancies.[94] It is found that the formation of oxygen vacancies increases the carrier concentration and photocurrent (Figure 7c and d). In addition, the author proved for the first time that an extra electron in $BiFeO_3$ spontaneously locates on $Fe^{3+}$ ion to form a small polaron. The formation of small polarons disturbs the valence state and generates additional localized states above the VBM of the original $BiFeO_3$ (Figure 7a and b). The results show that the main reason why oxygen vacancies can improve the performance of PEC is that it can be used as a donor to increase the carrier concentration of $BiFeO_3$.

$BiFeO_3$ is a typical ferroelectric material with large, stable and adjustable ferroelectric polarization, which can generate a depolarizing electric field inside the electrode and extend to the surface of the film, so that the photogenerated electrons and holes are effectively separated.[95] In 2013, Yao and colleagues used a simple sputtering deposition method to synthesize $BiFeO_3$ films with ferroelectric effects.[96] Studies find that when it is used in water splitting photoanodes, significant anode photocurrent is observed, which can realize unassisted PEC water splitting. In addition, the authors find that film thickness and iron polarization in different directions will affect the PEC performance. Thinner film and the negative charge on the film surface will cause the negative shift of the starting potential.

In addition, the existence of the ferroelectric domain makes $BiFeO_3$ have adjustable internal field orientation and intensity. When different applied voltages are applied, in theory, a single ferroelectric photoelectrode can be regarded as a photoanode

  

DOI: 10.14102/j.cnki.0254-5861.2021-0020

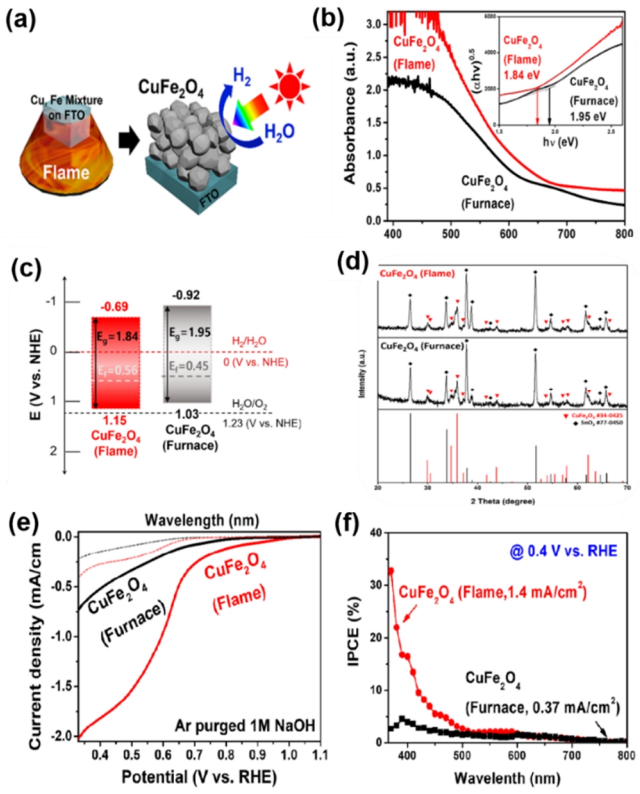


**Figure 8.** (a) Illustration of the flame annealing conditions and the porous film structure of the flame-annealed $CuFe_2O_4$ on FTO. (b) UV-vis spectra and the corresponding Tauc plots for indirect bandgaps shown in insets. (c) Comparison of the energy band positions for $CuFe_2O_4$ annealed by furnace and flame in contact with aqueous electrolyte at pH 0. (d) XRD spectra of $CuFe_2O_4$ film on FTO annealed by flame (top) and furnace (middle). (e) J-V curves of $CuFe_2O_4$ photocathode measured in Ar purged 1 M NaOH. (f) IPCE of $CuFe_2O_4$ photocathode. Reproduced with permission from Ref.[107]

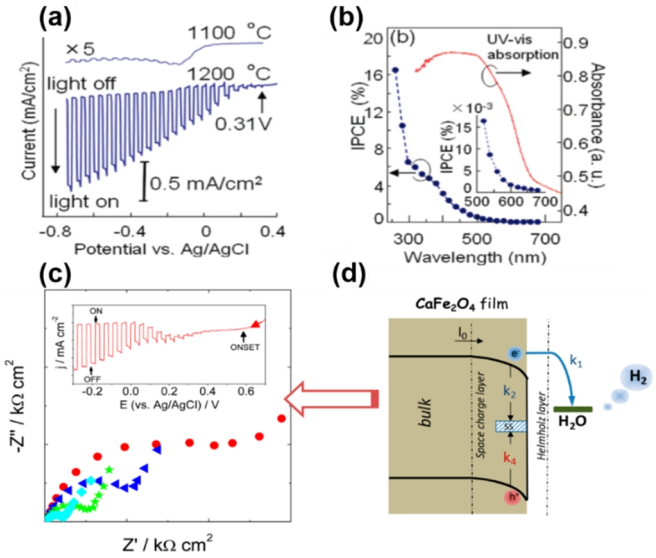


**Figure 9.** (a) Current-potential curves in 0.1 M NaOH solution under chopped light illumination (500 W Xe lamp) for $CaFe_2O_4$ electrodes treated at 1200 and 1100 °C. (b) IPCE spectrum of $CaFe_2O_4$ electrodes treated at 1200 °C with –0.8 V vs Ag/AgCl in 0.1 M NaOH and UV-vis absorption spectrum of $CaFe_2O_4$. Reproduced with permission from Ref.[114] (c) Experimental Nyquist plots in $N_2$-purged 0.1 M $Na_2SO_4$ at a constant applied potential of 0 V vs. Ag/AgCl and different $e\Phi_0$, (d) Electron transport mechanism. Reproduced with permission from Ref.[110]

and a photocathode respectively when different internal field orientations are applied. Lei et al. used spin coating technology to prepare polycrystalline ferroelectric $BiFeO_3$ photoelectrodes, and studied the influence of polarization pretreatment on the bend orientation of the $BiFeO_3$ band.[97] At 0 V vs. Ag/AgCl electrode, when the polarization bias of the pretreatment is changed from –8 V to +8 V, the photocurrent can be switched from 0 to 10 mA·cm$^{-2}$, and the open circuit potential can be changed from 33 to 440 mV. The results show that the polarization pretreatment of $BiFeO_3$ makes it possible to manipulate the photoelectrochemical reaction on a single ferroelectric photoelectric, and provides insights for the design of smart PEC systems. PEC performance of ferrite photoanodes are compared in Table 1.

## Ferrite Photocathode for Water Reduction

**$CuFe_2O_4$.** Spinel $CuFe_2O_4$ is used as an attractive p-type photocathode in PEC water splitting. Theoretically, the maximum photocurrent density of $CuFe_2O_4$ that can be generated is 27 mA·cm$^{-2}$, and the maximum solar-hydrogen conversion efficiency is 33%. $CuFe_2O_4$ has merit of narrow band gap (1.3–1.5 eV), low cost, high mechanical strength, easy synthesis, and good stability. Roy and colleagues prepared a highly porous $CuFe_2O_4$ nanoarray photocathode material using a low-temperature surfactant-assisted solvent thermal phase change induced temperature-controlled etching process.[29,105] After PEC measurement, the IPCE of the $CuFe_2O_4$ sample synthesized at 180 °C with $\delta$ = 0.77 was 18.7%, which is higher than that of the photocathode with $\delta$ = 0.71. This study emphasizes the effect of phase and morphology control on PEC performance and proves the application of solvothermal etching in causing phase changes, which provides valuable references for other porous ferrites used in PEC water splitting research.

Although $CuFe_2O_4$ has excellent photoelectric performance, the photocurrent is still very low when it is used solely as a photocathode material. This is mainly due to the severe photogenerated electron-hole recombination of $CuFe_2O_4$ material, which greatly inhibits its photocatalytic performance. Researchers used various modification methods such as doping, introducing oxygen vacancy, and constructing of heterojunctions, to change the surface and interface structure of the material to improve the serious problem of photo-generated electron-hole recombination in $CuFe_2O_4$ materials. Nadeem et al. reported the deposition of $CuFe_2O_4$/$\alpha$-$Fe_2O_3$ composite film on FTO glass.[106] Since the conduction band of $CuFe_2O_4$ is quite different from the redox potential of $H_2O/H_2$, the author combined it with n-type $\alpha$-$Fe_2O_3$, which leads to light excited electrons flow from the conduction band of $\alpha$-$Fe_2O_3$ to the valence band of $CuFe_2O_4$, and promote the separation of photogenerated electrons and hole pairs through the Z-type path. Another reason for the poor PEC performance of the $CuFe_2O_4$ photocathode is the contact between the $CuFe_2O_4$ film and the FTO conductive glass. The crystallization temperature of $CuFe_2O_4$ is generally 800−1000 °C, while the glass transition temperature of FTO is about 564 °C. The annealing in the furnace

  

DOI: 10.14102/j.cnki.0254-5861.2021-0020

**Table 2.** Comparison of PEC Performance, Onset Potential and Preparation of Different Ferrite Photocathode for Water Reduction

| Ferrite photocathode | Electrolyte | J (1.23 V vs RHE) | $V_{onset}$ ($V_{RHE}$) | Preparation | Reference |
|---|---|---|---|---|---|
| Ag-doped $CaFe_2O_4$ | 0.2 M $K_2SO_4$ | 1.2 mA·cm$^{-2}$ at −0.6 V vs Ag/AgCl | 0.36 V vs Ag/AgCl | radio frequency (RF) magnetron cosputtering | [108] |
| $Co_3O_4$ loaded $CaFe_2O_4$/$\alpha$-$Fe_2O_3$ | 1.0 M NaOH (pH = 13.6) | 75 μA·cm$^{-2}$ | 0.6 | electrodeposition | [109] |
| $CaFe_2O_4$ | 0.1 M $Na_2SO_4$ (pH = 6) | −0.38 mA·cm$^{-2}$ at −0.2 V vs Ag/AgCl | 0.4 V vs Ag/AgCl | sol-gel method | [110] |
| p-$CaFe_2O_4$/n-$Fe_2O_3$ | 1.0 M NaOH | 0.53 mA·cm$^{-2}$ | 0.7 | hydrothermal method | [111] |
| $CaFe_2O_4$/$BiVO_4$ | 0.5 M $Na_2SO_4$ (Ph = 6.5) | 0.96 mA·cm$^{-2}$ | 0.38 | electrophoretically deposited | [112] |
| $CaFe_2O_4$/TaON | 0.5 M NaOH (pH = 13.7) | 1.26 mA·cm$^{-2}$ | 0.7 | electrophoretic deposition | [113] |
| $CaFe_2O_4$ | 0.1 M NaOH | −0.7 mA·cm$^{-2}$ at −0.4 V vs Ag/AgCl | 0.3 V vs Ag/AgCl | solution method | [114] |
| $CuFe_2O_4$ | 1 M $H_2SO_4$ | −2.57 mA·cm$^2$ at −1 V vs RHE | 0.3 | solvothermal etching | [29] |
| $CuFe_2O_4$ (flame) | Ar purged 1 M NaOH | −1.82 mA·cm$^{-2}$ at 0.4 V vs RHE. | 1.0 | high-temperature flame annealing | [107] |
| $CuFe_2O_4$/$\alpha$-$Fe_2O_3$ | 1 M NaOH | 1.22 mA·cm$^{-2}$ | 0.95 | ultrasonic spray pyrolysis | [106] |
| $CuFe_2O_4$ | $N_2$ purged 0.1 M NaOH | −0.04 mA·cm$^{-2}$ at 0.4 V vs RHE. | 1.1 | electrodeposition | [115] |
| $CuFe_2O_4$ | 0.2 M $Na_2SO_4$ | −0.4 mA·cm$^{-2}$ at 0.4 V vs RHE. | 0.5 | hydrothermal method | [116] |
| p-$NiFe_2O_4$/n-$Fe_2O_3$ | 1 M NaOH | 2.1 mA·cm$^{-2}$ | 0.82 | ultrasonic spray pyrolysis | [117] |
| $LaFeO_3$ | 0.1 M KOH | 0.30 mA·cm$^{-2}$ at 1 V vs. Ag/AgCl | 0.25 V vs Ag/AgCl | sol-gel method | [118] |
| $LaFe_{0.9}Cu_{0.1}O_3$ | 0.1 M KOH | 0.99 mA·cm$^{-2}$ at 1 V vs. Ag/AgCl | 0.25 V vs Ag/AgCl | sol-gel method | [118] |
| $BiVO_4$/$LaFe_{0.5}Co_{0.5}O_3$ | 0.5 M KPi (pH = 7.0) | 3.4 mA·cm$^{-2}$ | 0.2 | electrodeposition | [119] |
| Au/$LaFeO_3$ | 0.1 M $Na_2SO_4$ | −19.60 mA·cm$^{-2}$ at 0.6 V vs. RHE | 1.0 | sol-gel method | [120] |
| $Fe_2O_3$/$LaFeO_3$ | 1 M NaOH | 0.97 mA·cm$^{-2}$ | 0.95 | aerosol spray pyrolysis method | [121] |
| k-$LaFeO_3$ | 0.1 M KOH (pH = 13) | −0.04 mA·cm$^{-2}$ | 1.2 | electrodeposition | [122] |

requires a long time, the contact between the film and the substrate after sintering is not good, and the glass substrate is easily damaged under high temperature conditions. Therefore, it is necessary to develop a new annealing method. Zheng et al. studied the potential of rapid flame annealing $CuFe_2O_4$ as a photocathode for PEC hydrogen production.[107] The sample prepared by this method has high crystallinity and good contact with the substrate, so it will not damage the substrate (Figure 8a and d). The SEM test observed that the flame-annealed $CuFe_2O_4$ film is thicker and has a porous structure, which leads to better light absorption and a larger surface area (Figure 8b and c). The photocurrent density of flame-annealed $CuFe_2O_4$ photocathode under 0.4 V vs. RHE is −1.82 mA·cm$^{-2}$, which is 3.5 times that of the furnace-annealed $CuFe_2O_4$ (0.52 mA·cm$^{-2}$) (Figure 8e and f). It is higher than the photocurrent density value of common copper-based ternary oxides and other photocathode ferrites without load (see table 2). This rapid flame annealing can also be used for the preparation of other ferrite films.

**$CaFe_2O_4$.** $CaFe_2O_4$ is one of the most studied water splitting ternary oxide photocathodes. It has a relatively narrow band gap (1.9 eV), can absorb visible light, and also has a band edge position suitable for water splitting. In 1987, Matsumoto et al. reported for the first time that $CaFe_2O_4$ was used as a photocathode material for PEC water splitting.[123] However, similar to the aforementioned $CuFe_2O_4$, due to the rapid charge recombination and the high temperature required for electrode preparation, high temperature will cause severe sintering and damage the conductive substrate, so its activity and practical application are greatly limited. Ida et al. prepared a (hk0)-oriented p-type $CaFe_2O_4$ photocathode, which showed relatively high PEC water splitting performance[114]. The PEC performance test showed that the electrode calcined at 1200 °C showed a higher photocurrent density and IPCE value than 1100 °C calcined (Figure 9 a and b). This research provides a theoretical reference for improving the quality of other complex ferrite films.

In addition to improving the contact surface between the film and the FTO conductive glass, efficient PEC water splitting also relies on effective charge transfer at the semiconductor/solution interface.[124] Gomez et al. prepared a thin-film $CaFe_2O_4$ electrode and studied the PEC mechanism of hydrogen production by electrochemical impedance spectroscopy (EIS)[110] (Figure 9c). Interestingly, the author concluded through theory and experiment that the existence of the surface state in $CaFe_2O_4$ is the center of electron capture and recombination, and electrons are directly transferred from the conduction band to water when hydrogen is produced (Figure 9d). This strategy of studying the mechanism of water splitting reaction through EIS can also provide an effective reference for the modification of other complex ferrites.

Recently, Yamaguchi and colleagues synthesized the orthorhombic octahedral $CaFe_2O_4$, and tested it in an alkaline environment

  

DOI: 10.14102/j.cnki.0254-5861.2021-0020

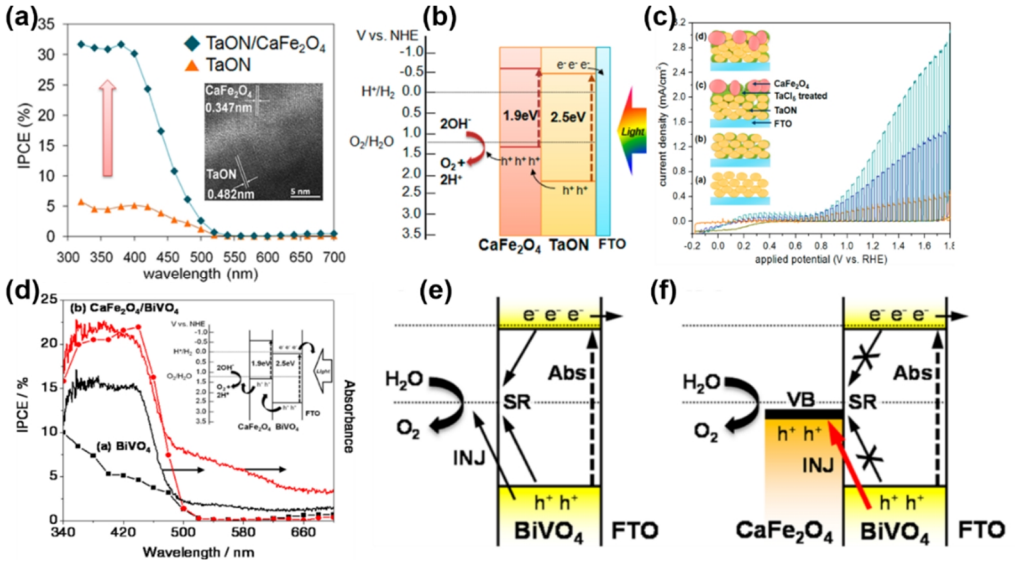


**Figure 10.** (a) IPCE of TaON-treated electrode (triangle) and TaON-as deposited/$CaFe_2O_4$ electrode (diamond). The inset shows interface between TaON and $CaFe_2O_4$ layers. (b) Energy diagram and expected charge flow of heterojunction photoanode. Reproduced with permission from Ref.[113] (c) Photocurrent density in 0.5 M NaOH under chopped light irradiation ($\lambda$ > 420 nm). (d) IPCE of a) $BiVO_4$ and b) $CaFe_2O_4/BiVO_4$ electrodes and their absorption spectra. Inset shows the energy diagram and expected charge flow of $CaFe_2O_4/BiVO_4$ heterojunction photoanode. Schematic diagrams illustrate the reaction at the surface of (e) $BiVO_4$ and (f) $CaFe_2O_4/BiVO_4$ photoanodes. Reproduced with permission from Ref.[112]

to prove its efficient and stable electrocatalytic OER performance. DFT calculations showed that the oxygen intermediates in $CaFe_2O_4$ directly form O–O bonds and are adsorbed in the Fe active sites. This is an important reason for the improvement of its OER performance.[125]

Similar to other p-type ferrites, $CaFe_2O_4$ has lower photoelectric conversion efficiency when used as a single photocatalytic cathode. Therefore, researchers mostly combine $CaFe_2O_4$ with other bandgap-matched semiconductors to construct heterojunctions.[126] For example, Parida et al. prepared p-$CaFe_2O_4$@n-$ZnFe_2O_4$ heterojunction and studied its photocatalytic performance.[127] Wang and colleagues prepared a-$Fe_2O_3$/$CaFe_2O_4$ p-n heterojunction for the photodegradation of organic matter.[128] Lee et al. uniformly load $CaFe_2O_4$ on TaON film by electrophoretic deposition to form a heterojunction (Figure 10b).[113] PEC test results show that enhanced light absorption leads to a substantial increase in IPCE (Figure 10a). The nearly 5-fold increase in photocurrent density (Figure 10c) is attributed to reduced carrier transport resistance and enhanced charge separation efficiency.

Similarly, Lee et al. successfully loaded $CaFe_2O_4$ on a $BiVO_3$ film and formed a staggered type II heterojunction structure[112] (Figure 10e and f). Under the simulated sunlight of 100 mW·cm$^{-2}$, the composite photoelectrode shows a higher photocurrent and stability, and the enhanced light absorption makes the IPCE value as high as 23% (Figure 10d). The formation of heterojunction reduces the charge recombination on the electrode surface and enhances the transfer efficiency of photo-generated holes.

Metal doping has also been studied as an effective strategy for adjusting energy bands and enhancing light absorption. Morikawa et al. used radio frequency magnetron sputtering to prepare p-type $CaFe_2O_4$ semiconductors doped with CuO, Au and Ag.[108] Studies have found that the doping of CuO and Au can broaden the light absorption range and generate plasmon resonance to increase the photocurrent density. However, it can be seen from the XRD test that doping reduces the symmetry of the structure and the crystallinity of $CaFe_2O_4$ (Figure 11a and b). Interestingly, Ag doping changes the twisted crystal structure of $CaFe_2O_4$, thus causing a red shift in light absorption and resulting in a nearly 23-fold increase in photocurrent (Figure 11c).

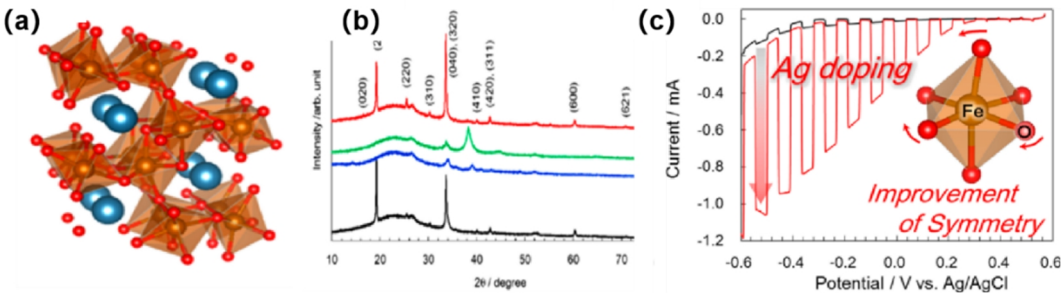


**Figure 11.** (a) Crystal structure of $CaFe_2O_4$ (Ca, blue; Fe, brown; O, red), (b) XRD patterns, (c) Current-potential curves measured in $O_2$-saturated 0.2 M $K_2SO_4$ solution under chopped light irradiation (300−800 nm) for Ag (35 W)-$CaFe_2O_4$ (red line). The electrodes were post annealed at 927 K, and the film thickness was fixed at ca.180 nm. Reproduced with permission from Ref.[108]


DOI: 10.14102/j.cnki.0254-5861.2021-0020

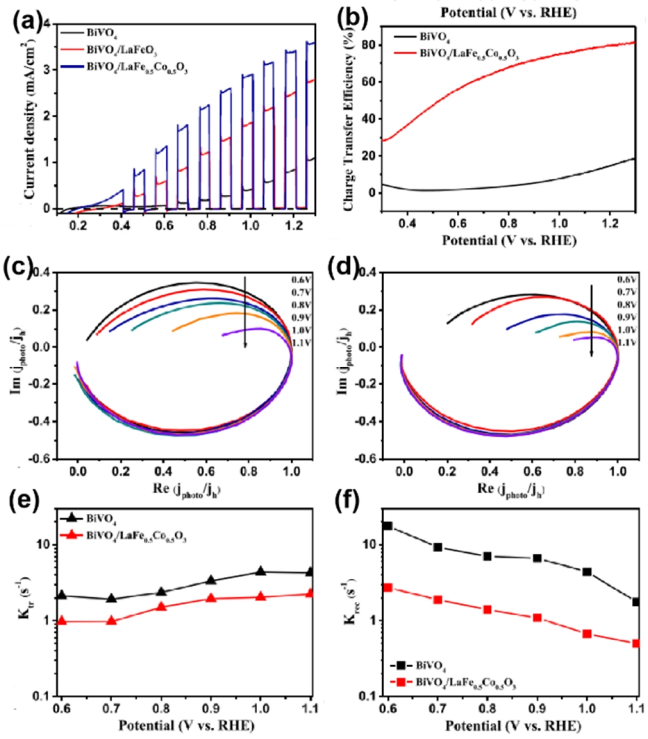


**Figure 12.** (a) J-V curves of $BiVO_4$ and $BiVO_4/LaFe_{0.5}Co_{0.5}O_3$ photoanodes (0.5 M KPi buffer solution, pH = 7.0) under chopped AM 1.5G illumination. (b) Charge transfer efficiencies of bare $BiVO_4$ and $BiVO_4/LaFe_{0.5}Co_{0.5}O_3$. (c) IMPS spectra of $BiVO_4$. (d) IMPS spectra of $BiVO_4/LaFe_{0.5}Co_{0.5}O_3$. (e) Charge transfer rate constant and (f) Recombination rate constant for $BiVO_4$ and $BiVO_4/LaFe_{0.5}Co_{0.5}O_3$. Reproduced with permission from Ref.[119]

**$LaFeO_3$.** Lanthanum ferrite ($LaFeO_3$) is a typical rare earth composite metal oxide with a perovskite ($ABO_3$) structure. Due to its stable crystal structure, non-toxicity, suitable band gap energy, unique catalysis and gas sensitivity, it is widely used in magnetic sensors,[129] electrical,[130] and industrial catalysis.[131] With the development of society and high and new technology, thin film materials have become an important branch in the field of materials science with their unique properties. $LaFeO_3$ films are an important class of functional thin film materials in typical $ABO_3$ composite structures.

The redox reactions involved in the perovskite-type thermochemical cycle are as follows:

$$ABO_3 \rightarrow ABO_{3-\delta} + (\delta/2)O_2\,(g)\ (1)$$

$$ABO_{3-\delta} + \delta H_2O\,(g) \rightarrow ABO_3 + \delta H_2\,(g)\ (2)$$

$$ABO_{3-\delta} + \delta CO_2\,(g) \rightarrow ABO_3 + \delta CO\,(g)\ (3)$$

Due to its suitable conduction and valence band positions across the entire water redox potential, abundant storage capacity, and stable photo-corrosion resistance, $LaFeO_3$ stands out in a series of p-type semiconductor materials. The main limitation of $LaFeO_3$ photocathode is the considerable bulk electron-hole recombination. Elemental doping can effectively increase the majority carrier density and improve its catalytic performance. In practical applications, various aspects of materials are generally improved by doping various elements.[48,132,133]

Choi and colleagues combined theoretical and experimental studies to explore the effect of K-doped La site in $LaFeO_3$ on its catalytic performance.[122] Theoretical and experimental studies have shown that K-doping produces shallower acceptor levels above the VBM of $LaFeO_3$, and can effectively increase the density of most carriers, reduce the recombination rate of electrons and holes, and enhance its charge transmission performance and stable photocurrent.

Recently, Ge et al. synthesized $LaFeO_3$, $BiVO_4/LaFeO_3$ and $BiVO_4/LaFe_{0.5}Co_{0.5}O_3$ using a simple electrochemical deposition method.[119] Co-substituted $LaFeO_3$ as a co-catalyst significantly improved water splitting performance. Compared with pure $BiVO_4$, the water oxidation photocurrent of $BiVO_4$/Co-$LaFeO_3$ composite photoanode is 3.4 $mA \cdot cm^{-2}$ at 1.23 V vs. RHE, which is about 4 times higher than that of pure $BiVO_4$, accompanied by a significant cathodic potential shift of 300 mV (Figure 12a). Combined with optical and electrochemical characterization, the addition of co-$LaFeO_3$ can significantly improve the electrolyte charge transfer efficiency of $BiVO_4$ (Figure 12b). From the study of intensity-modulated photocurrent spectroscopy on the surface dynamics of carriers, it is observed that the surface recombination rate constant is suppressed (Figure 12c–f), which can attribute the enhancement of its PEC water splitting performance.

In summary, $LaFeO_3$'s excellent stability and suitable band gap position make it widely used in photocatalysis. It has been found that doping with metal elements can increase the carrier concentration. Future research should start from controlling the doping concentration, and using the band gap advantage to form composite materials with other semiconductors, combining multiple modification strategies to effectively improve PEC water decomposition performance.

## n CONCLUSIONS AND OUTLOOK

In short, due to its unique crystal structure, excellent electromagnetic, catalytic and gas sensitivity advantages, ferrite has gradually become a hot research material at home and abroad. With the continuous progress of thin film preparation technology, the application field of ferrite is also continuously expanded, and its preparation and modification methods are also continuously improved. On the whole, the material is still in the stage of continuous research and development, and the amount of relevant scientific literature is still relatively small. This article summarized some shortcomings of ferrite itself and corresponding improvement strategies: (1) The sintering situation is serious when used for photocatalysis. Researchers have developed many modification strategies to improve their PEC activity, such as controlling the formation and nano-morphology of thin-film materials as mentioned in the article. Since most complex ferrites need to be calcined in a high temperature environment, and the degree of contact between the film material and the conductive glass substrate will affect its photoelectric catalytic performance. Future research in this area should be devoted to the development of more efficient and energy-saving calcining methods, improve the contact between the film material and the conductive substrate without destroying the conductive substrate. The size effect, surface effect and other characteristics of nanomaterials require us to more accurately control the morphology of thin film materials, and to develop more accurate test instruments for characterization. (2) The visible light response is weak. Ferrite materials have poor electrical conductivity and low light absorption efficiency. At present, doping is mainly used to control the carrier concentration and increase the electrical conductivity. However, the mechanism

  

DOI: 10.14102/j.cnki.0254-5861.2021-0020

of the energy band change caused by doping to broaden the light absorption is still unclear. Future research should focus on regulating the doping concentration, conducting in-depth analysis of structural changes caused by different changes, and proposing possible theoretical mechanisms. (3) The recombination of photogenerated electrons and holes is serious. Surface modification and construction of heterojunctions to improve the efficiency of charge transfer have been studied to improve the catalytic performance of ferrites. Due to the adjustable electronic structure of ferrites and suitable band gaps, they can be combined with other semiconductors. On one hand, the surface can be modified, and on the other hand, the charge separation can be increased. The photoelectric catalytic water splitting catalysts developed at present all have low conversion efficiency. In the future, more efficient and low-cost catalysts should be developed. These need to be further explored by researchers.

## n ACKNOWLEDGEMENTS

This work was financially supported by the National Natural Science Foundation of China (21808189, 52173277), National Natural Science Foundation of Gansu province (No. 20JR5RA523), and the Young Teachers' Research Ability Improvement Project of Northwest Normal University (NWNU-LKQN2020-01).

## n AUTHOR INFORMATION

Corresponding author. Email: wangqizhao@163.com, qizhaosjtu@gmail.com (Q.Wang)

## n COMPETING INTERESTS

The authors declare no competing interests.

## n ADDITIONAL INFORMATION

Supplementary information is available for this paper at http://manu30.magtech.com.cn/jghx/EN/10.14102/j.cnki.0254-5861.2021-0020

For submission: https://mc03.manuscriptcentral.com/cjsc

## n REFERENCES

(1) Yan, Y.; Fang, Q.; Pan, J.; Yang, J.; Zhang, L.; Zhang, W.; Zhuang, G.; Zhong, X.; Deng, S.; Wang, J. Efficient photocatalytic reduction of $CO_2$ using Fe-based covalent triazine frameworks decorated with in situ grown $ZnFe_2O_4$ nanoparticles. *Chem. Eng. J.* **2021**, 408, 127358.

(2) Wang, L.; Huang, G.; Zhang, L.; Lian, R.; Huang, J.; She, H.; Liu, C.; Wang, Q. Construction of $TiO_2$-covalent organic framework Z-scheme hybrid through coordination bond for photocatalytic $CO_2$ conversion. *J. Energy Chem.* **2022**, 64, 85–92.

(3) Zhou, S.; Chen, K.; Huang, J.; Wang, L.; Zhang, M.; Bai, B.; Liu, H.; Wang, Q. Preparation of heterometallic CoNi-MOFs-modified $BiVO_4$: a steady photoanode for improved performance in photoelectrochemical water splitting. *Appl. Catal. B: Environ.* **2020**, 266, 118513.

(4) Huang, J.; Du, X.; Feng, Y.; Zhao, Y.; Ding, Y. New insights into water oxidation reactions from photocatalysis, electrocatalysis to chemical catalysis: an example of iron-based oxides doped with foreign elements. *Phys. Chem. Chem. Phys.* **2016**, 18, 9918–9921.

(5) Han, J.; Liu, Z. Optimization and modulation strategies of zinc oxide-based photoanodes for highly efficient photoelectrochemical water splitting. *ACS Appl. Energy Mater.* **2021**, 4, 1004–1013.

(6) Han, H.; Yang, Y.; Liu, J.; Zheng, X.; Wang, X.; Meng, S.; Zhang, S.; Fu, X.; Chen, S. Effect of Zn vacancies in $Zn_3In_2S_6$ nanosheets on boosting photocatalytic $N_2$ fixation. *ACS Appl. Energy Mater.* **2020**, 3, 11275–11284.

(7) Jang, Y.; Lindberg, A.; Lumley, M.; Choi, K. Photoelectrochemical nitrogen reduction to ammonia on cupric and cuprous oxide photocathodes. *ACS Energy Lett.* **2020**, 5, 1834–1839.

(8) Takalkar, G.; Bhosale, R. R.; AlMomani, F.; Kumar, A.; Banu, A.; Ashok, A.; Rashid, S.; Khraisheh, M.; Shakoor, A.; al Ashraf, A. Thermochemical splitting of $CO_2$ using solution combustion synthesized $LaMO_3$ (where, M = Co, Fe, Mn, Ni, Al, Cr, Sr). *Appl. Surf. Sci.* **2020**, 509, 144908.

(9) Gao, Z.; Chen, K.; Wang, L.; Bai, B.; Liu, H.; Wang, Q. Aminated flower-like $ZnIn_2S_4$ coupled with benzoic acid modified g-$C_3N_4$ nanosheets via covalent bonds for ameliorated photocatalytic hydrogen generation. *Appl. Catal. B: Environ.* **2020**, 268, 118462.

(10) Chen, Y.; Xu, M.; Wen, J.; Wan, Y.; Zhao, Q.; Cao, X.; Ding, Y.; Wang, Z. L.; Li, H.; Bian, Z. Selective recovery of precious metals through photocatalysis. *Nat. Sustain* **2021**, 4, 618–626.

(11) Fujishima, A.; Honda, K. Electrochemical photolysis of water at a semiconductor electrode. *Nature* **1972**, 238, 37–38.

(12) Huang, J.; Liu, T.; Wang, R.; Zhang, M.; Wang, L.; She, H.; Wang, Q. Facile loading of cobalt oxide on bismuth vanadate: proved construction of p-n junction for efficient photoelectrochemical water oxidation. *J. Colloid Interf. Sci.* **2020**, 570, 89–98.

(13) Yue, P.; She, H.; Zhang, L.; Niu, B.; Lian, R.; Huang, J.; Wang, L.; Wang, Q. Super-hydrophilic CoAl-LDH on $BiVO_4$ for enhanced photoelectrochemical water oxidation activity. *Appl. Catal. B: Environ.* **2021**, 286, 119875.

(14) Zhou, P.; Yu, J.; Jaroniec, M. All-solid-state Z-scheme photocatalytic systems. *Adv. Mater.* **2014**, 26, 4920–4935.

(15) Guo, Z.; Liu, Z. Synthesis and control strategies of nanomaterials for photoelectrochemical water splitting. *Dalton Trans.* **2021**, 50, 1983–1989.

(16) Wen, P.; Sun, Y.; Li, H.; Liang, Z.; Wu, H.; Zhang, J.; Zeng, H.; Geyer, S. M.; Jiang, L. A highly active three-dimensional Z-scheme ZnO/Au/g-$C_3N_4$ photocathode for efficient photoelectrochemical water splitting. *Appl. Catal. B: Environ.* **2020**, 263, 118180.

(17) Jian, S.; Tian, Z.; Hu, J.; Zhang, K.; Zhang, L.; Duan, G.; Yang, W.; Jiang, S. Enhanced visible light photocatalytic efficiency of La-doped ZnO nanofibers via electrospinning-calcination technology. *Adv. Powder Mater.* **2021**.

(18) She, H.; Yue, P.; Ma, X.; Huang, J.; Wang, L.; Wang, Q. Fabrication of $BiVO_4$ photoanode cocatalyzed with NiCo-layered double hydroxide for enhanced photoactivity of water oxidation. *Appl. Catal. B: Environ.* **2020**, 263, 118280.

(19) Huang, J.; Wang, Y.; Chen, K.; Liu, T.; Wang, Q. Boosting the photoelectrochemical water oxidation performance of bismuth vanadate by $ZnCo_2O_4$ nanoparticles. *Chin. Chem. Lett.* **2021**, 6664.

(20) Zhou, S.; Yue, P.; Huang, J.; Wang, L.; She, H.; Wang, Q. High-performance photoelectrochemical water splitting of $BiVO_4$@Co-MIm prepared by a facile in-situ deposition method. *Chem. Eng. J.* **2019**, 371, 885–892.

(21) Fang, M.; Qin, Q.; Cai, Q.; Liu, W. Transparent $Co_3FeO_x$ film passivated $BiVO_4$ photoanode for efficient photoelectrochemical water splitting. *Chin. J. Struct. Chem.* **2021**, 35, 0254–5861.

(22) Li, H.; Wang, T.; Liu, S.; Luo, Z.; Li, L.; Wang, H.; Zhao, Z. J.; Gong, J. Controllable distribution of oxygen vacancies in grain boundaries of p-Si/$TiO_2$ heterojunction photocathodes for solar water splitting. *Angew. Chem. Int. Ed.* **2021**, 60, 4034–4037.

(23) Xiao, J.; Huang, H.; Huang, Q.; Li, X.; Hou, X.; Zhao, L.; Ma, R.; Chen, H.; Li, Y. Remarkable improvement of the turn-on characteristics of a $Fe_2O_3$ photoanode for photoelectrochemical water splitting with coating

  

DOI: 10.14102/j.cnki.0254-5861.2021-0020

a FeCoW oxy-hydroxide gel. *Appl. Catal. B: Environ.* **2017**, 212, 89–96.
(24) Pan, Z.; Zhang, G.; Wang, X. Polymeric carbon nitride/reduced graphene oxide/$Fe_2O_3$: all-solid-state Z-scheme system for photocatalytic overall qater aplitting. *Angew. Chem. Int. Ed.* **2019**, 58, 7102–7106.
(25) Zheng, G.; Wang, J.; Zu, G.; Che, H.; Lai, C.; Li, H.; Murugadoss, V.; Yan, C.; Fan, J.; Guo, Z. Sandwich structured $WO_3$ nanoplatelets for highly efficient photoelectrochemical water splitting. *J. Mater. Chem. A* **2019**, 7, 26077–26088.
(26) Jelinska, A.; Bienkowski, K.; Jadwiszczak, M.; Pisarek, M.; Strawski, M.; Kurzydlowski, D.; Solarska, R.; Augustynski, J. Enhanced photocatalytic water splitting on very thin $WO_3$ films activated by high-temperature annealing. *ACS Catal.* **2018**, 8, 10573–10580.
(27) Huang, J.; Yue, P.; Wang, L.; She, H.; Wang, Q. A review on tungsten-trioxide-based photoanodes for water oxidation. *Chin. J. Catal.* **2019**, 40, 1408–1420.
(28) Huang, J.; Ding, Y.; Luo, X.; Feng, Y. Solvation effect promoted formation of p–n junction between $WO_3$ and FeOOH: a high performance photoanode for water oxidation. *J. Catal.* **2016**, 333, 200–206.
(29) Maitra, S.; Pal, S.; Maitra, T.; Halder, S.; Roy, S. Solvothermal etching-assisted phase and morphology tailoring in highly porous $CuFe_2O_4$ nanoflake photocathodes for solar water splitting. *Energ. Fuel.* **2021**, 35, 14087–14100.
(30) Xu, H.; Liu, T.; Bai, S.; Li, L.; Zhu, Y.; Wang, J.; Yang, S.; Li, Y.; Shao, Q.; Huang, X. Cation exchange strategy to single-atom noble-metal doped CuO nanowire arrays with ultralow overpotential for $H_2O$ splitting. *Nano Lett.* **2020**, 20, 5482–5489.
(31) Soltani, T.; Tayyebi, A.; Lee, B. K. $BiFeO_3/BiVO_4$ p−n heterojunction for efficient and stable photocatalytic and photoelectrochemical water splitting under visible-light irradiation. *Catal. Today* **2020**, 340, 188–196.
(32) Song, J.; Kim, T. L.; Lee, J.; Cho, S. Y.; Cha, J.; Jeong, S. Y.; An, H.; Kim, W. S.; Jung, Y. S.; Park, J.; Jung, G. Y.; Kim, D.; Jo, J.; Bu, S.; Jang, H.; Lee, S. Domain-engineered $BiFeO_3$ thin-film photoanodes for highly enhanced ferroelectric solar water splitting. *Nano Res.* **2017**, 11, 642–655.
(33) Li, C.; He, J.; Xiao, Y.; Li, Y.; Delaunay, J. J. Earth-abundant Cu-based metal oxide photocathodes for photoelectrochemical water splitting. *Energy Environ. Sci.* **2020**, 13, 3269–3306.
(34) Li, J.; Chen, H.; Triana, C. A.; Patzke, G. R. Hematite photoanodes for water oxidation: electronic transitions, carrier dynamics, and surface energetics. *Angew. Chem. Int. Ed.* **2021**, 60, 18380–18396.
(35) Narang, S. B.; Pubby, K. Nickel spinel ferrites: a review. *J. Magn. Magn. Mater.* **2021**, 519, 167163.
(36) Sun, C.; Alonso, J. A.; Bian, J. Recent advances in perovskite-type oxides for energy conversion and storage applications. *Adv. Energy Mater.* **2020**, 11, 2000459.
(37) Lee, D.; Lee, D.; Lumley, M.; Choi, K. Progress on ternary oxide-based photoanodes for use in photoelectrochemical cells for solar water splitting. *Chem. Soc. Rev.* **2019**, 48, 2126–2157.
(38) Shen, X.; Yao, M.; Sun, K.; Zhao, T.; He, Y.; Chi, C. Y.; Zhou, C.; Dapkus, P. D.; Lewis, N. S.; Hu, S. Defect-tolerant $TiO_2$-coated and discretized photoanodes for >600 h of stable photoelectrochemical water oxidation. *ACS Energy Lett.* **2020**, 6, 193–200.
(39) Huang, J.; Hu, G.; Ding, Y.; Pang, M.; Ma, B. Mn-doping and NiFe layered double hydroxide coating: effective approaches to enhancing the performance of $\alpha$-$Fe_2O_3$ in photoelectrochemical water oxidation. *J. Catal.* **2016**, 340, 261–269.
(40) Özgür, Ü.; Alivov, Y.; Morkoç, H. Microwave ferrites, part 1: fundamental properties. *J. Mater. Sci-Mater El.* **2009**, 20, 789–834.
(41) Issa, B.; Obaidat, I. M.; Albiss, B. A.; Haik, Y. Magnetic nanoparticles: surface effects and properties related to biomedicine applications. *Int. J. Mol. Sci.* **2013**, 14, 21266–21305.
(42) Amiri, M.; Salavati-Niasari, M.; Akbari, A. Magnetic nanocarriers: evolution of spinel ferrites for medical applications. *Adv. Colloid Interface Sci.* **2019**, 265, 29–44.
(43) Lan, Y.; Liu, Z.; Guo, Z.; Ruan, M.; Xin, Y. Accelerating the charge separation of $ZnFe_2O_4$ nanorods by Cu–Sn ions gradient doping for efficient photoelectrochemical water splitting. *J. Colloid Interf. Sci.* **2019**, 552, 111–121.
(44) Fu, Y.; Dong, C.; Zhou, W.; Lu, Y.; Huang, Y.; Liu, Y.; Guo, P.; Zhao, L.; Chou, W.; Shen, S. A ternary nanostructured $\alpha$-$Fe_2O_3$/Au/$TiO_2$ photoanode with reconstructed interfaces for efficient photoelectrocatalytic water splitting. *Appl. Catal. B: Environ.* **2020**, 260, 118206.
(45) Wang, D.; Han, D.; Shi, Z.; Wang, J.; Yang, J.; Li, X.; Song, H. Optimized design of three-dimensional multi-shell $Fe_3O_4/SiO_2$/ZnO/ZnSe microspheres with type II heterostructure for photocatalytic applications. *Appl. Catal. B: Environ.* **2018**, 227, 61–69.
(46) Zhang, Z.; Hua, Z.; Lang, J.; Song, Y.; Zhang, Q.; Han, Q.; Fan, H.; Gao, M.; Li, X.; Yang, J. Eco-friendly nanostructured Zn–Al layered double hydroxide photocatalysts with enhanced photocatalytic activity. *Cryst.Eng.Comm* **2019**, 21, 4607–4619.
(47) Triyono, D.; Hanifah, U.; Laysandra, H. Structural and optical properties of Mg-substituted $LaFeO_3$ nanoparticles prepared by a sol-gel method. *Results Phys.* **2020**, 16.
(48) Andrei, F.; Boerasu, I.; Birjega, R.; Moldovan, A.; Dinescu, M.; Ion, V.; Mihailescu, C.; Scarisoreanu, N. D.; Leca, V. The effects of the oxygen content on the photoelectrochemical properties of $LaFeO_3$ perovskite thin films obtained by pulsed laser deposition. *Appl. Phys. A-Mater.* **2019**, 125, 125–807.
(49) Phan, T.; Nikoloski, A.; Bahri, P.; Li, D. Optimizing photocatalytic performance of hydrothermally synthesized $LaFeO_3$ by tuning material properties and operating conditions. *J. Environ. Chem. Eng.* **2018**, 6, 1209–1218.
(50) Freeman, E.; Kumar, S.; Celorrio, V.; Park, M. S.; Kim, J. H.; Fermin, D. J.; Eslava, S. Strategies for the deposition of $LaFeO_3$ photocathodes: improving the photocurrent with a polymer template. *Sustain. Energ. Fuels* **2020**, 4, 884–894.
(51) Compton, J. S.; Peterson, C. A.; Dervishogullari, D.; Sharpe, L. R. Spray pyrolysis as a combinatorial method for the generation of photocatalyst libraries. *ACS Comb. Sci.* **2019**, 21, 489–499.
(52) Lanfredi, S.; Storti, F.; Simões, L. P. M.; Djurado, E.; Nobre, M. A. L. Synthesis and structural characterization of calcium titanate by spray pyrolysis method. *Mater. Lett.* **2017**, 201, 148–151.
(53) Guo, Y.; Zhang, N.; Wang, X.; Qian, Q.; Zhang, S.; Li, Z.; Zou, Z. A facile spray pyrolysis method to prepare Ti-doped $ZnFe_2O_4$ for boosting photoelectrochemical water splitting. *J. Mater. Chem. A* **2017**, 5, 7571–7577.
(54) Chen, H.; Mulmudi, H. K.; Tricoli, A. Flame spray pyrolysis for the one-step fabrication of transition metal oxide films: recent progress in electrochemical and photoelectrochemical water splitting. *Chin. Chem. Lett.* **2020**, 31, 601–604.
(55) Stoerzinger, K.; Wang, L.; Ye, Y.; Bowden, M.; Crumlin, E. J.; Du, Y.; Chambers, S. A. Linking surface chemistry to photovoltage in Sr-substituted $LaFeO_3$ for water oxidation. *J. Mater. Chem. A* **2018**, 6, 22170–22178.
(56) Xu, K.; Feng, J. Superior photocatalytic performance of $LaFeO_3$/g-$C_3N_4$ heterojunction nanocomposites under visible light irradiation. *RSC Adv.* **2017**, 7, 45369–45376.
(57) Zhang, Y.; Ding, J.; Xu, W.; Wang, M.; Shao, R.; Sun, Y.; Lin, B. Mesoporous $LaFeO_3$ perovskite derived from MOF gel for all-solid-state symmetric supercapacitors. *Chem. Eng. J.* **2020**, 386, 124030.
(58) Azouzi, W.; Sigle, W.; Labrim, H.; Benaissa, M. Sol-gel synthesis of

  

DOI: 10.14102/j.cnki.0254-5861.2021-0020

nanoporous $LaFeO_3$ powders for solar applications. *Mater. Sci. Semicond. Process.* **2019**, 104, 104682.

(59) Pawar, G.; Elikkottil, A.; Pesala, B.; Tahir, A.; Mallick, T. Plasmonic nickel nanoparticles decorated on to $LaFeO_3$ photocathode for enhanced solar hydrogen generation. *Int. J. Hydrogen Energy* **2019**, 44, 578–586.

(60) Li, Y.; Hu, Y.; Fang, T.; Li, Z.; Zou, Z. Promoted photoelectrochemical activity of $BiVO_4$ coupled with $LaFeO_3$ and $LaCoO_3$. *Res. Chem. Intermediat* **2017**, 44, 1013–1024.

(61) Wang, X.; Li, Y.; Zhang, X.; Li, J.; Li, X.; Wang, C. Design and fabrication of NiS/$LaFeO_3$ heterostructures for high efficient photodegradation of organic dyes. *Appl. Surf. Sci.* **2020**, 504, 144363.

(62) Mesbah, M.; Hamedshahraki, S.; Ahmadi, S.; Sharifi, M.; Igwegbe, C. A. Hydrothermal synthesis of $LaFeO_3$ nanoparticles adsorbent: characterization and application of error functions for adsorption of fluoride. *MethodsX* **2020**, 7, 100786.

(63) Iervolino, G.; Vaiano, V.; Sannino, D.; Rizzo, L.; Palma, V. Enhanced photocatalytic hydrogen production from glucose aqueous matrices on Ru-doped $LaFeO_3$. *Appl. Catal. B: Environ.* **2017**, 207, 182–194.

(64) Keerthana, S.; Yuvakkumar, R.; Ravi, G.; Pavithra, S.; Thambidurai, M.; Dang, C.; Velauthapillai, D. Pure and Ce-doped spinel $CuFe_2O_4$ photocatalysts for efficient rhodamine B degradation. *Environ. Res.* **2021**, 200, 111528.

(65) Liang, Q.; Jin, J.; Liu, C.; Xu, S.; Li, Z. Constructing a novel p-n heterojunction photocatalyst $LaFeO_3$/g-$C_3N_4$ with enhanced visible-light-driven photocatalytic activity. *J. Alloy. Compd.* **2017**, 709, 542–548.

(66) Zhu, Z.; Peelaers, H.; Van de Walle, C. G. Electronic and protonic conduction in $LaFeO_3$. *J. Mater. Chem. A* **2017**, 5, 15367–15379.

(67) Ye, Y.; Yang, H.; Li, R.; Wang, X. Enhanced photocatalytic performance and mechanism of Ag-decorated $LaFeO_3$ nanoparticles. *J. Sol-gel. Sci. Techn.* **2017**, 82, 509–518.

(68) Vasile, E.; Sima, M.; Sima, A.; Logofatu, C. $TiO_2$/$Fe_2O_3$ photoanodes for solar water oxidation prepared via electrodeposition of amorphous precursors. *Mater. Res. Bull.* **2020**, 121, 110623.

(69) Ghahramanifard, F.; Rouhollahi, A.; Fazlolahzadeh, O. Electrodeposition of Cu-doped p-type ZnO nanorods; effect of Cu doping on structural, optical and photoelectrocatalytic property of ZnO nanostructure. *Superlattices Microstruct.* **2018**, 114, 1–14.

(70) Henning, R.; Uredat, P.; Simon, C.; Bloesser, A.; Cop, P.; Elm, M.; Marschall, R. Characterization of $MFe_2O_4$ (M = Mg, Zn) thin films prepared by pulsed laser deposition for photoelectrochemical applications. *J. Phys. Chem. C* **2019**, 123, 18240–18247.

(71) Wheeler, G.; Choi, K. Photoelectrochemical properties and stability of nanoporous p-type $LaFeO_3$ photoelectrodes prepared by electrodeposition. *ACS Energy Lett.* **2017**, 2, 2378–2382.

(72) Qin, J.; Cui, Z.; Yang, X.; Zhu, S.; Li, Z.; Liang, Y. Synthesis of three-dimensionally ordered macroporous $LaFeO_3$ with enhanced methanol gas sensing properties. *Sensor Actuat. B: Chem.* **2015**, 209, 706–713.

(73) Song, P.; Zhang, H.; Han, D.; Li, J.; Yang, Z.; Wang, Q. Preparation of biomorphic porous $LaFeO_3$ by sorghum straw biotemplate method and its acetone sensing properties. *Sensor Actuat. B: Chem.* **2014**, 196, 140–146.

(74) Khan, I.; Sun, N.; Wang, Y.; Li, Z.; Qu, Y.; Jing, L. Synthesis of $SnO_2$/yolk-shell $LaFeO_3$ nanocomposites as efficient visible-light photocatalysts for 2,4-dichlorophenol degradation. *Mater. Res. Bull.* **2020**, 127, 110857.

(75) Huang, K.; Liu, J.; Wang, L.; Chang, G.; Wang, R.; Lei, M.; Wang, Y.; He, Y. Mixed valence CoCuMnO*x* spinel nanoparticles by sacrificial template method with enhanced ORR performance. *Appl. Surf. Sci.* **2019**, 487, 1145–1151.

(76) Qu, Y.; Zhang, Z.; Du, K.; Chen, W.; Lai, Y.; Liu, Y.; Li, J. Synthesis of nitrogen-containing hollow carbon microspheres by a modified template method as anodes for advanced sodium-ion batteries. *Carbon* **2016**, 105, 103–112.

(77) Peng, Z.; Liu, X.; Meng, H.; Li, Z.; Li, B.; Liu, Z.; Liu, S. Design and tailoring of the 3D macroporous hydrous $RuO_2$ hierarchical architectures with a hard-template method for high-performance supercapacitors. *ACS Appl. Mater. Inter.* **2017**, 9, 4577–4586.

(78) Simon, C.; Timm, J.; Tetzlaff, D.; Jungmann, J.; Apfel, U. P.; Marschall, R. Mesoporous $NiFe_2O_4$ with tunable pore morphology for electrocatalytic water oxidation. *ChemElectroChem* **2021**, 8, 227–239.

(79) Su, H.; Jing, L.; Shi, K.; Yao, C.; Fu, H. Synthesis of large surface area $LaFeO_3$ nanoparticles by SBA-16 template method as high active visible photocatalysts. *J. Nanopart. Res.* **2009**, 12, 967–974.

(80) Kim, J.; Kim, J.; Kim, J.; Kim, Y.; Lee, J. Intentional extrinsic doping into $ZnFe_2O_4$ nanorod photoanode for enhanced photoelectrochemical water splitting. *Solar RRL* **2019**, 4, 1900328.

(81) Zhu, X.; Guijarro, N.; Liu, Y.; Schouwink, P.; Wells, R. A.; Le Formal, F.; Sun, S.; Gao, C.; Sivula, K. Spinel structural disorder influences solar-water-splitting performance of $ZnFe_2O_4$ nanorod photoanodes. *Adv. Mater.* **2018**, 1801612.

(82) Gao, W.; Peng, R.; Yang, Y.; Zhao, X.; Cui, C.; Su, X.; Qin, W.; Dai, Y.; Ma, Y.; Liu, H.; Sang, Y. Electron spin polarization-enhanced photoinduced charge separation in ferromagnetic $ZnFe_2O_4$. *ACS Energy Lett.* **2021**, 6, 2129–2137.

(83) Wang, J.; Wang, Y.; Xv, X.; Chen, Y.; Yang, X.; Zhou, J.; Li, S.; Cao, F.; Qin, G. Defective $Fe^{3+}$ self-doped spinel $ZnFe_2O_4$ with oxygen vacancies for highly efficient photoelectrochemical water splitting. *Dalton Trans.* **2019**, 48, 11934–11940.

(84) Hou, Y.; Li, X.; Zhao, Q.; Quan, X.; Chen, G. Electrochemical method for synthesis of a $ZnFe_2O_4$/$TiO_2$ composite nanotube array modified electrode with enhanced photoelectrochemical activity. *Adv. Funct. Mater.* **2010,** 20, 2165–2174.

(85) Long, J.; Wang, W.; Fu, S.; Liu, L. Hierarchical architectures of wrinkle-like $ZnFe_2O_4$ nanosheet-enwrapped ZnO nanotube arrays for remarkably photoelectrochemical water splitting to produce hydrogen. *J. Colloid Interf. Sci.* **2019**, 536, 408–413.

(86) McDonald, K. D.; Bartlett, B. M. Microwave synthesis of spinel $MgFe_2O_4$ nanoparticles and the effect of annealing on photocatalysis. *Inorg. Chem.* **2021**, 60, 8704–8709.

(87) Jin, P.; Wang, L.; Ma, X.; Lian, R.; Huang, J.; She, H.; Zhang, M.; Wang, Q. Construction of hierarchical $ZnIn_2S_4$@PCN-224 heterojunction for boosting photocatalytic performance in hydrogen production and degradation of tetracycline hydrochloride. *Appl. Catal. B: Environ.* **2021**, 284, 119762.

(88) Hou, Y.; Zuo, F.; Dagg, A.; Feng, P. A three-dimensional branched cobalt-doped alpha-$Fe_2O_3$ nanorod/$MgFe_2O_4$ heterojunction array as a flexible photoanode for efficient photoelectrochemical water oxidation. *Angew. Chem. Int. Ed.* **2013**, 52, 1248–1252.

(89) Jia, J.; Du, X.; Zhang, Q.; Liu, E.; Fan, J. Z-scheme $MgFe_2O_4$/$Bi_2MoO_6$ heterojunction photocatalyst with enhanced visible light photocatalytic activity for malachite green removal. *Appl. Surf. Sci.* **2019**, 492, 527–539.

(90) Fan, W.; Li, M.; Bai, H.; Xu, D.; Chen, C.; Li, C.; Ge, Y.; Shi, W. Fabrication of $MgFe_2O_4$/$MoS_2$ heterostructure nanowires for photoelectrochemical catalysis. *Langmuir* **2016**, 32, 1629–1636.

(91) Batoo, K. M.; Kumar, G.; Yang, Y.; Al-Douri, Y.; Singh, M.; Jotania, R. B.; Imran, A. Structural, morphological and electrical properties of $Cd^{2+}$ doped $MgFe_{2-x}O_4$ ferrite nanoparticles. *J. Alloy. Compd.* **2017**, 726, 179–186.

(92) Kumar, G. M.; Cho, H. D.; Lee, D. J.; Kumar, J. R.; Siva, C.;

  

DOI: 10.14102/j.cnki.0254-5861.2021-0020

Ilanchezhiyan, P.; Kim, D. Y.; Kang, T. W. Elevating the charge separation of $MgFe_2O_4$ nanostructures by Zn ions for enhanced photocatalytic and photoelectrochemical water splitting. *Chemosphere* **2021**, 283, 131134.

(93) Yan, X.; Pu, R.; Xie, R.; Zhang, B.; Shi, Y.; Liu, W.; Ma, G.; Yang, N. Design and fabrication of $Bi_2O_3$/$BiFeO_3$ heterojunction film with improved photoelectrochemical performance. *Appl. Surf. Sci.* **2021**, 552, 149442.

(94) Radmilovic, A.; Smart, T. J.; Ping, Y.; Choi, K. S. Combined experimental and theoretical investigations of n-type $BiFeO_3$ for use as a photoanode in a photoelectrochemical cell. *Chem. Mater.* **2020**, 32, 3262–3270.

(95) Müller, M.; Huang, Y. L.; Vélez, S.; Ramesh, R.; Fiebig, M.; Trassin, M. Training the polarization in integrated $La_{0.15}Bi_{0.85}FeO_3$-based devices. *Adv. Mater.* 2104688.

(96) Ji, W.; Yao, K.; Lim, Y. F.; Liang, Y. C.; Suwardi, A. Epitaxial ferroelectric $BiFeO_3$ thin films for unassisted photocatalytic water splitting. *Appl. Phys. Lett.* **2013**, 103, 062901.

(97) Cao, D.; Wang, Z.; Nasori; Wen, L.; Mi, Y.; Lei, Y. Switchable charge-transfer in the photoelectrochemical energy-conversion process of ferroelectric $BiFeO_3$ photoelectrodes. *Angew. Chem. Int. Ed.* **2014**, 53, 11027–11031.

(98) Liu, Y.; Xia, M.; Yao, L.; Mensi, M.; Ren, D.; Grätzel, M.; Sivula, K.; Guijarro, N. Spectroelectrochemical and chemical evidence of surface passivation at zinc ferrite ($ZnFe_2O_4$) photoanodes for solar water oxidation. *Adv. Funct. Mater.* **2021**, 2010081.

(99) Kim, J.; Jang, Y.; Kim, J.; Jang, J.; Choi, S.; Lee, J. Defective $ZnFe_2O_4$ nanorods with oxygen vacancy for photoelectrochemical water splitting. *Nanoscale* **2015**, 7, 19144–19151.

(100) Guijarro, N.; Bornoz, P.; Prévot, M.; Yu, X.; Zhu, X.; Johnson, M.; Jeanbourquin, X.; Le Formal, F.; Sivula, K. Evaluating spinel ferrites $MFe_2O_4$ (M = Cu, Mg, Zn) as photoanodes for solar water oxidation: prospects and limitations. *Sustain. Energ. Fuels* **2018**, 2, 103–117.

(101) Khoomortezaei, S.; Abdizadeh, H.; Golobostanfard, M. R. Ferro-photocatalytic enhancement of photoelectrochemical water splitting using the $WO_3$/$BiFeO_3$ heterojunction. *Energ. Fuel.* **2021**, 35, 9623–9634.

(102) Soltani, T.; Lee, B. K. Ag-doped $BiVO_4$/$BiFeO_3$ photoanode for highly efficient and stable photocatalytic and photoelectrochemical water splitting. *Sci. Total. Environ.* **2020**, 736, 138640.

(103) Wu, X.; Li, H.; Wang, X.; Jiang, L.; Xi, J.; Du, G.; Ji, Z. Ferroelectric enhanced photoelectrochemical water splitting in $BiFeO_3$/$TiO_2$ composite photoanode. *J. Alloy. Compd.* **2019**, 783, 643–651.

(104) Khoomortezaei, S.; Abdizadeh, H.; Golobostanfard, M. R. Triple layer heterojunction $WO_3$/$BiVO_4$/$BiFeO_3$ porous photoanode for efficient photoelectrochemical water splitting. *ACS Appl. Energy Mater.* **2019**, 2, 6428–6439.

(105) Yu, Y. Y.; Zhang, H. Q. Reduced graphene oxide coupled magnetic $CuFe_2O_4$-$TiO_2$ nanoparticles with enhanced photocatalytic activity for methylene blue degradation. *Chin. J. Struct. Chem.* **2016**, 35, 472–480.

(106) Hussain, S.; Hussain, S.; Waleed, A.; Tavakoli, M.; Wang, Z.; Yang, S.; Fan, Z.; Nadeem, M. A. Fabrication of $CuFe_2O_4$/alpha-$Fe_2O_3$ composite thin films on FTO coated glass and 3-D nanospike structures for efficient photoelectrochemical water splitting. *ACS Appl. Mater. Interfaces* **2016**, 8, 35315–35322.

(107) Park, S.; Baek, J.; Zhang, L.; Lee, J. M.; Stone, K. H.; Cho, I. S.; Guo, J.; Jung, H. S.; Zheng, X. Rapid flame-annealed $CuFe_2O_4$ as efficient photocathode for photoelectrochemical hydrogen production. *ACS Sustain. Chem. Eng.* **2019**, 7, 5867–5874.

(108) Sekizawa, K.; Nonaka, T.; Arai, T.; Morikawa, T. Structural improvement of $CaFe_2O_4$ by metal doping toward enhanced cathodic photocurrent. *ACS Appl. Mater. Interfaces* **2014**, 6, 10969–10973.

(109) Cai, J.; Li, S.; Qin, G. Interface engineering of $Co_3O_4$ loaded $CaFe_2O_4$/$Fe_2O_3$ heterojunction for photoelectrochemical water oxidation. *Appl. Surf. Sci.* **2019,** 466, 92–98.

(110) Diez-Garcia, M. I.; Gomez, R. Investigating water splitting with $CaFe_2O_4$ photocathodes by electrochemical impedance spectroscopy. *ACS Appl. Mater. Interfaces* **2016**, 8, 21387–21397.

(111) Ahmed, M. G.; Kandiel, T. A.; Ahmed, A. Y.; Kretschmer, I.; Rashwan, F.; Bahnemann, D. Enhanced photoelectrochemical water oxidation on nanostructured hematite photoanodes via p-$CaFe_2O_4$/n-$Fe_2O_3$ heterojunction formation. *J. Phys. Chem. C* **2015**, 119, 5864–5871.

(112) Kim, E.; Kang, H.; Magesh, G.; Kim, J.; Jang, J.; Lee, J. Improved photoelectrochemical activity of $CaFe_2O_4$/$BiVO_4$ heterojunction photoanode by reduced surface recombination in solar water oxidation. *ACS Appl. Mater. Interfaces* **2014**, 6, 17762–11769.

(113) Kim, E.; Nishimura, N.; Magesh, G.; Kim, J.; Jang, J.; Jun, H.; Kubota, J.; Domen, K.; Lee, J. Fabrication of $CaFe_2O_4$/TaON heterojunction photoanode for photoelectrochemical water oxidation. *J. Am. Chem. Soc.* **2013**, 135, 5375–5383.

(114) Ida, S.; Yamada, K.; Matsunaga, T.; Hagiwara, H.; Matsumoto, Y.; Ishihara, T. Preparation of p-type $CaFe_2O_4$ photocathodes for producing hydrogen from water. *J. Am. Chem. Soc.* **2010**, 132, 17343–17345.

(115) Diez-Garcia, M.; Lana-Villarreal, T.; Gomez, R. Study of copper ferrite as a novel photocathode for water reduction: improving its photoactivity by electrochemical pretreatment. *ChemSusChem* **2016**, 9, 1504–1512.

(116) Li, X.; Liu, A.; Chu, D.; Zhang, C.; Du, Y.; Huang, J.; Yang, P. High performance of manganese porphyrin sensitized p-type $CuFe_2O_4$ photocathode for solar water splitting to produce hydrogen in a tandem photoelectrochemical cell. *Catalysts* **2018**, 8, 2073–4344.

(117) Hussain, S.; Tavakoli, M. M.; Waleed, A.; Virk, U. S.; Yang, S.; Waseem, A.; Fan, Z.; Nadeem, M. A. Nanotextured spikes of alpha-$Fe_2O_3$/$NiFe_2O_4$ composite for efficient photoelectrochemical oxidation of water. *Langmuir* **2018**, 34, 3555–3564.

(118) Peng, Q.; Shan, B.; Wen, Y.; Chen, R. Enhanced charge transport of $LaFeO_3$ via transition metal (Mn, Co, Cu) doping for visible light photoelectrochemical water oxidation. *Int. J. Hydrogen Energy* **2015**, 40, 15423–15431.

(119) Gao, Y.; Yang, G.; Dai, Y.; Li, X.; Gao, J.; Li, N.; Qiu, P.; Ge, L. Electrodeposited Co-substituted $LaFeO_3$ for enhancing the photoelectrochemical activity of $BiVO_4$. *ACS Appl. Mater. Interfaces* **2020**, 12, 17364–17375.

(120) Wang, P.; He, Y.; Mi, Y.; Zhu, J.; Zhang, F.; Liu, Y.; Yang, Y.; Chen, M.; Cao, D. Enhanced photoelectrochemical performance of $LaFeO_3$ photocathode with Au buffer layer. *RSC Adv.* **2019**, 9, 26780–26786.

(121) Fang, T.; Guo, Y.; Cai, S.; Zhang, N.; Hu, Y.; Zhang, S.; Li, Z.; Zou, Z. Improved charge separation efficiency of hematite photoanodes by coating an ultrathin p-type $LaFeO_3$ overlayer. *Nanotechnology* **2017**, 28, 394003.

(122) Wheeler, G. P.; Baltazar, V. U.; Smart, T. J.; Radmilovic, A.; Ping, Y.; Choi, K. S. Combined theoretical and experimental investigations of atomic doping to enhance photon absorption and carrier transport of $LaFeO_3$ photocathodes. *Chem. Mater.* **2019**, 31, 5890–5899.

(123) Matsumoto, Y.; Omae, M.; Sugiyama, K.; Sato, E. New photocatho-de materials for hydrogen evolution: $CaFe_2O_4$ and $Sr_7Fe_{10}O_{22}$. *J. Phys. Chem.* **1986**, 91, 577–581.

(124) Kumar Das, A.; Srinivasan, A. Structural transition and associated magnetic properties of heat treated electrospun one-dimensional $CaFe_2O_4$. *Chem. Phys. Lett.* **2022**, 786.

(125) Sugawara, Y.; Kamata, K.; Ishikawa, A.; Tateyama, Y.; Yamaguchi, T. Efficient oxygen evolution electrocatalysis on $CaFe_2O_4$ and its reaction mechanism. *ACS Appl. Energy Mater.* **2021**, 4, 3057–3066.

  

DOI: 10.14102/j.cnki.0254-5861.2021-0020

(126) Xiao, G. A new inorganic-organic hybrid based on biisoquinoline and hexachloridostannate: structure, photoluminescence, electrochemical behavior and theoretical study. *Chin. J. Struct. Chem.* **2014**, 33, 1689–1696.

(127) Behera, A.; Kandi, D.; Martha, S.; Parida, K. Constructive interfacial charge carrier separation of a p-$CaFe_2O_4$@n-$ZnFe_2O_4$ heterojunction architect photocatalyst toward photodegradation of antibiotics. *Inorg. Chem.* **2019**, 58, 16592–16608.

(128) Wang, J.; Xu, X.; Cao, F.; Wang, Y.; Li, S.; Qin, G. In situ fabrication of *α*-$Fe_2O_3$/$CaFe_2O_4$ p-n heterojunction with enhanced VOCs photodegradation activity. *Adv. Powder Technol.* **2019**, 30, 590–595.

(129) Hao, P.; Qiu, G.; Song, P.; Yang, Z.; Wang, Q. Construction of porous $LaFeO_3$ microspheres decorated with NiO nanosheets for high response ethanol gas sensors. *Appl. Surf. Sci.* **2020**, 515, 146025.

(130) Li, K. Y.; Wang, D. J.; Wu, F. Q.; Xie, T. F.; Li, T. J. Studies on photoelectric gas-sensitive characters of nanocrystalline $LaFeO_3$. *Mater. Chem. Phys.* **1999**, 60, 226–230.

(131) Yu, J.; Xiang, S.; Ge, M.; Zhang, Z.; Huang, J.; Tang, Y.; Sun, L.; Lin, C.; Lai, Y. Rational construction of $LaFeO_3$ perovskite nanoparticle-modified $TiO_2$ nanotube arrays for visible-light driven photocatalytic activity. *Coatings* **2018**, 8, 374.

(132) Lin, Q.; Lin, J.; Yang, X.; He, Y.; Wang, L.; Dong, J. The effects of $Mg^{2+}$ and $Ba^{2+}$ dopants on the microstructure and magnetic properties of doubly-doped $LaFeO_3$ perovskite catalytic nanocrystals. *Ceram. Int.* **2019**, 45, 3333–3340.

(133) Xu, N.; Li, F.; Gao, L.; Hu, H.; Hu, Y.; Long, X.; Ma, J.; Jin, J. N. Cu-Codoped carbon nanosheet/Au/$CuBi_2O_4$ photocathodes for efficient photoelectrochemical water splitting. *ACS Sustain. Chem. Eng.* **2018**, 6, 7257–7264.

Received: 29 October, 2021
Accepted: 1 December, 2021
Published: January 13, 2022

  

DOI: 10.14102/j.cnki.0254-5861.2021-0020